

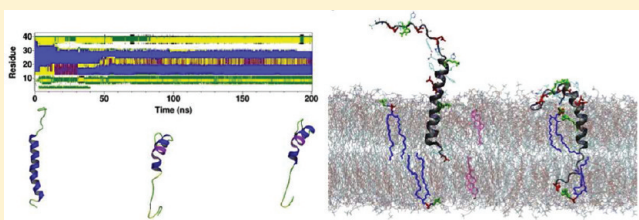
Molecular Dynamics Simulations Reveal the Protective Role of Cholesterol in β -Amyloid Protein-Induced Membrane Disruptions in Neuronal Membrane Mimics

Liming Qiu,[†] Creighton Buie,^{†,‡} Andrew Reay,[‡] Mark W. Vaughn,[‡] and Kwan Hon Cheng^{*,†}

[†]Department of Physics and [‡]Department of Chemical Engineering, Texas Tech University, Lubbock, Texas 79409, United States

 Supporting Information

ABSTRACT: Interactions of β -amyloid ($A\beta$) peptides with neuronal membranes have been associated with the pathogenesis of Alzheimer's disease (AD); however, the molecular details remain unclear. We used atomistic molecular dynamics (MD) simulations to study the interactions of $A\beta_{40}$ and $A\beta_{42}$ with model neuronal membranes. The differences between cholesterol-enriched and depleted lipid domains were investigated by the use of model phosphatidylcholine (PC) lipid bilayers with and without 40 mol % cholesterol. A total of 16 independent 200 ns simulation replicates were investigated. The surface area per lipid, bilayer thickness, water permeability barrier, and lipid order parameter, which are sensitive indicators of membrane disruption, were significantly altered by the inserted state of the protein. We conclude that cholesterol protects $A\beta$ -induced membrane disruption and inhibits β -sheet formation of $A\beta$ on the lipid bilayer. The latter could represent a two-dimensional (2D) seeding template for the formation of toxic oligomeric $A\beta$ in the pathogenesis of AD.



1. INTRODUCTION

Alzheimer's disease (AD) is a neurological disorder that progressively impairs memory and cognitive capability of patients.¹ The presence of extracellular amyloid deposits, or plaques on neuronal membranes, is a significant histological or diagnostic marker of AD.^{2,3} A major component of these plaques is a self-aggregated fibrillar form of β -amyloid ($A\beta$), a short 39–42 residue amphiphilic peptide of ~ 4 kDa.³ Monomeric $A\beta$ is released upon a highly regulated sequential proteolytic cleavage of the large 100 kDa transmembrane amyloid precursor protein (APP) by two proteases, β and γ secretases.³ The normal, nonpathological concentration of $A\beta$ in the extracellular matrix is subnanomolar, but its physiological role is unclear.^{2,4,5}

In vitro studies of $A\beta$ reveal that monomeric $A\beta$ adopts a largely random-coil structure^{6–8} in aqueous solution. At the nonphysiological micromolar concentration region, monomeric $A\beta$ peptides rapidly unfold and self-aggregate to form soluble protofibrils or oligomers that are toxic to neurons.³ The detailed structure of these oligomers and the factors regulating their formation are still unknown.² According to the amyloid cascade hypothesis,^{2,9} self-aggregation of $A\beta$ into toxic oligomers is a critical event in the pathogenesis of AD. The key factors that modulate the interaction of monomeric or oligomeric $A\beta$ with the neuronal membrane, a major site of the $A\beta$ deposit formation,⁹ remain unclear. At present, early lipid membrane interaction events of monomeric $A\beta$, between its release from the parent APP and before the toxic oligomer formation, are difficult to access either experimentally or computationally.

Experimentally, the major challenge lies in the preparation of structurally homogeneous, monomeric $A\beta$ samples in solution or

in lipid membranes. This difficulty stems from the peptide's propensity to spontaneously form mesoscopic oligomers.¹⁰ Computationally, only the NMR-structure of $A\beta_{40}$ in micelles,¹¹ a lipid membrane-mimic, is currently available. However, the primary structures of $A\beta_{40}$ and $A\beta_{42}$, the 40 and 42 residue-long major $A\beta$ peptides, are known.^{2,11,12} Significant progress in the computational study of the $A\beta$ interactions with membranes requires a computationally robust and biologically relevant multicomponent lipid/water membrane nanodomain model. The model system should capture the structures and dynamics of key lipid components with high atomic resolution. Several lipid models of well-defined organizations and/or compositions have been proposed.^{13–17} Most current studies of $A\beta$ /membrane interactions use small single-component lipid membranes.^{18–26} However, accumulative experimental evidence suggests that lipids in cell membranes are not randomly distributed but exhibit highly ordered cholesterol-enriched nanodomains known as "lipid rafts" that are surrounded by disordered cholesterol-depleted lipid matrix, or "non-lipid raft regions".^{15,27–33} Therefore, these single-component lipid bilayer models may not provide useful information regarding the conformational transitions of membrane-active peptide structures and their disruptive effects in membranes.

This computational study used phosphatidylcholine (PC) and PC/cholesterol (PC/CHOL) bilayers to mimic the cholesterol-depleted and enriched lipid domains of neuronal membranes. We focused on the interactions of $A\beta_{40}$ and $A\beta_{42}$ with these lipid

Received: February 8, 2011

Revised: June 17, 2011

Published: July 11, 2011

domains in a preinserted state, which represents a possible initial orientation state of $\text{A}\beta$ immediately upon its release from the APP by the secretases.¹¹ We have examined the protein insertion efficiency, protein unfolding, and protein-induced membrane disruption. The latter was characterized by the calculated water permeability barrier, transbilayer lipid polar group distribution, and order parameters of both PC acyl chains and cholesterol rings. Our results reveal a protective role of cholesterol in preventing both $\text{A}\beta$ -induced membrane disruption and membrane surface-induced β -sheet formation. The latter is important because surface-induced β -sheet formation may provide a template for the formation of toxic oligomeric $\text{A}\beta$ that further leads to the pathogenesis of AD.

2. MATERIALS AND METHODS

2.1. $\text{A}\beta$ Primary Structures. The primary sequence of $\text{A}\beta_{40}$ and $\text{A}\beta_{42}$ are known and shown here.³ Both peptides share the same first 40 residues, but the $\text{A}\beta_{42}$ contain two extra residues, ILE and ALA: H-Asp-Ala-Glu-Phe-Arg-His-Asp-Ser-Gly-Tyr-Glu-Val-His-His-Gln-Lys-Leu-Val-Phe-Phe-Ala-Glu-Asp-Val-Gly-Ser-Asn-Lys-Gly-Ala-Ile-Ile-Gly-Leu-Met-Val-Gly-Gly-Val-Val-(ILE-ALA)-OH.

2.2. Simulations of $\text{A}\beta$ in Cholesterol-Depleted and Enriched Membranes. The simulation systems consisted of four different protein/lipid/water/ion complexes: (A) $\text{A}\beta_{40}$ in PC, (B) $\text{A}\beta_{42}$ in PC, (C) $\text{A}\beta_{40}$ in PC/CHOL, and (D) $\text{A}\beta_{42}$ in PC/CHOL. All simulations were in the presence of explicit water and counterions. We used a 1-palmitoyl-2-oleoyl-PC with a saturated *sn*-1 chain (16:0) and an unsaturated *sn*-2 chain (18:1) for our PC lipid. Four independent replicates, each with a different initial velocity distribution but identical initial coordinates of the lipid and protein atoms, were generated for each series. Each replicate of a given series was denoted by a number running from 1 to 4. In total 16 replicates were generated: A1–A4, B1–B4, C1–C4, and D1–D4. In addition, eight extra independent “control replicates”, four of pure PC and four of pure PC/CHOL, were generated to provide protein-free controls. Each system was simulated for 200 ns, for a grand total of 4800 ns for the 24 trajectories generated in this study.

$\text{A}\beta_{40}$, for the A and C series, or $\text{A}\beta_{42}$, for the B and D series, was preinserted into the upper layer of a lipid bilayer. This system was intended to mimic the initial configuration of the protein with respect to neuronal cell membrane right after its enzymatic cleavage from its precursor APP.¹¹ The initial membrane structure was constructed of four identical smaller equilibrated PC or PC/CHOL lipid bilayers from a previous publication.³⁴ $\text{A}\beta$ proteins were then inserted into these initial structures. For the A and B series in which a protein was inserted into a pure PC membrane, a void was created by removing two PC molecules in the upper layer from the original structure. One protein molecule, $\text{A}\beta_{40}$, for A series, or $\text{A}\beta_{42}$, for B series, was inserted into this void. This new structure underwent energy minimization in vacuum to remove energetically unfavorable close contacts between the protein and lipid molecules. The energy-minimized structure was subsequently solvated in a water box then underwent energy minimization again in the presence of solvent. This was followed by a 100 ps simulation on the solvated system in which each atom of the protein or lipid molecule was position-restrained by coupling to its current position with a spring constant of 5000 $\text{kJ nm}^{-2} \text{ mol}^{-1}$. The above preparation procedures were effective in preventing the system from structurally disruptive shock at the beginning of each production run due

to local incomplete solvation. The procedures for preparing the C and D series were similar, except that two PC and one CHOL molecules were removed before the protein preinsertion.

The final structures from the preparative procedures described above were taken as the initial structures for the 200 ns production runs. The initial system size of the simulation box was $13.57 \times 14.80 \times 11.59 \text{ nm}^3$ for the A series, $13.24 \times 14.44 \times 11.71 \text{ nm}^3$ for the B series, $13.82 \times 15.98 \times 14.40 \text{ nm}^3$ for the C series, and $13.45 \times 15.55 \times 14.01 \text{ nm}^3$ for the D series. There were 574 PC molecules for the PC bilayers in the A and B series. There were 574 PC molecules and 383 cholesterol molecules for the PC/CHOL bilayers in the C and D series. To assess the effect of the $\text{A}\beta$ peptides on lipid membranes, control systems of PC and PC/CHOL lipid bilayers without the protein were constructed using identical preparative procedure but excluding the lipid removal and protein insertion steps. For the control systems, the initial simulation box was $13.30 \times 14.51 \times 13.26 \text{ nm}^3$ for the pure PC and $13.52 \times 15.64 \times 14.31 \text{ nm}^3$ for the PC/CHOL.

Molecular dynamics (MD) simulations of six different series, A–D series in the presence of protein and two pure lipid bilayer control series with no protein, were performed using the Gromacs 4.0 package^{35–38} with the GROMOS 87 force field and under constant number, pressure, and temperature (NPT) conditions. Periodic boundary conditions were applied to the *x*, *y*, and *z* directions for the whole system. Initial coordinates for POPC³⁴ and cholesterol³⁹ were obtained from published data with details given elsewhere.³⁴ A simple point charge (SPC) model⁴⁰ was employed for water. The nonbonded van de Waals interactions were estimated using a twin-range cutoff Lennard-Jones potential,³⁶ with interactions within 1.0 nm evaluated every step and interactions between 1.0 and 1.5 nm evaluated every 10 steps. Bond lengths were constrained by a linear constraint solver (LINCS) algorithm.⁴¹ Short-range electrostatic interactions were calculated with a smoothly shifted Coulomb potential,⁴² and long-range electrostatic interactions were approximated by a particle-mesh Ewald (PME) algorithm.^{43,44} A leapfrog integrator⁴⁵ was used for all systems with a 2 fs time step. Water, lipids, and protein in the simulation system were coupled separately to temperature baths of 300 K with a coupling time of 0.05 ps, using a v-rescale thermostat.^{42,46,47} Isotropic pressures of 1 atm were maintained through a Berendsen barostat⁴⁸ with a coupling time of 1 ps.

2.3. Data Analysis and Visualization. To analyze the membrane disruption due to the presence of protein, the lipids of each replicate were partitioned into two groups: the annular lipids (ALs) and the nonannular lipids (nALs).^{49,50} Here, ALs were defined as those lipids that were within 0.5 nm of the protein along the *x*–*y* plane and therefore confined to a cylinder-like column of irregular cross-section enclosing the protein. Lipids that were not ALs were nALs. See Section S1 in the Supporting Information (SI) for selection details.

2.3.1. Surface Areas of PC and Cholesterol. The average surface areas of PC (A_{PC}) and cholesterol (A_c) were calculated based on a method originally proposed by Hofsäss et al.⁵¹ with some modifications to take into account of the presence of the embedded protein. In our method, the total volume of the protein (v_p), the partial volume of the protein embedded in the lipid bilayer (v_p'), the average volume of PC (v_{PC}), and the average thickness of lipid bilayer (h) have to be estimated. The calculations and the assumptions used in the estimation of the protein and lipid parameters are given below.

A Monte Carlo integration method was used to calculate the total and partial protein volumes, that is, v_p and v_p' , respectively.

This method is similar to the estimation of the cross-section area (A) of the conformal AL column mentioned in the SI except that the integration was carried out in three dimensions for the volume calculation. The whole AL column was placed inside a three-dimensional (3D) rectangular box with a predetermined volume of V_B . Uniformly distributed random sampling points were generated inside this rectangular box. If the distance between a sampling point and any atom of the protein is less than twice the van der Waals radius of the atom under consideration, this sampling point is considered to be located inside the protein region. Although this cutoff distance, twice the van der Waals radius, of an atom of protein, may be arbitrary, this approach may take into account the void volume inside the α -helix barrel and the void volume between the protein and lipid molecules. Finally, v_p was estimated using the following equation

$$v_p \approx V_B \lim_{n \rightarrow \infty} \frac{n_{\text{protein}}}{n} \quad (1)$$

where n_{protein} is the number of sampling points inside the protein region, and n is the total number of sampling points. Error estimation is the same as in cross-section area calculation.

To calculate the partial volume v_p' , only those residues that satisfied the criterion of $z_p - z_c + r_{\text{VDW}} \geq 0$ were counted as the “embedded” residues inside the lipid bilayer. Here z_p and z_c are defined as the average z -position of the phosphorus (P8) of the PC in the upper layer and the exact z -position of the backbone carbon (C_α) of each residue of the protein, respectively, and r_{VDW} the van der Waals radius of the C_α . The use of approximately three million sample points ensured a precision of 3% with a 99% confidence interval, according to the worst-case sample size suggested by Fishman.⁵²

The average volume of PC (v_{PC}) was calculated by subtracting the volumes occupied by the water ($n_w v_w$), the cholesterol ($n_{\text{CHOL}} v_{\text{CHOL}}$), and the protein (v_p) from the volume of the AL or nAL region of interest (v_{ROI}) and then divided by n_{PC} as shown in eq 2 below. Here n_w , n_{CHOL} , and n_{PC} represent the numbers of water, CHOL, and PC within the v_{ROI} . Also, v_w and v_{CHOL} correspond to the estimated average volumes of water and cholesterol of 0.031546 and 0.593 nm³, respectively, from a recent study.⁵³

$$v_{\text{PC}} = \frac{v_{\text{ROI}} - v_p - n_w v_w - n_{\text{CHOL}} v_{\text{CHOL}}}{n_{\text{PC}}} \quad (2)$$

For nAL there is no protein, so the value of v_p is zero in eq 2.

The average thickness of the lipid bilayer (h) was obtained by dividing the volume of the lipid bilayer (v_{LB}) with or without the embedded protein segment with the cross-section area (A) of the region of interest, AL or nAL, as shown in eq 3. Here v_{LB} was estimated by subtracting the volumes occupied by the non-embedded protein ($v_p - v_p'$) and the water ($n_w v_w$).

$$h = \frac{v_{\text{LB}}}{A} = \frac{v_{\text{ROI}} - (v_p - v_p') - n_w v_w}{A} \quad (3)$$

For the case of nAL where the protein is not present, the value of ($v_p - v_p'$) is zero in eq 3.

Finally, the A_{PC} and A_{C} were deduced from the estimated v_{PC} (eq 2) and h (eq 3) as shown in eqs 4 and 5, respectively.

$$A_{\text{PC}} = \frac{2v_{\text{PC}}}{h} \quad (4)$$

$$A_{\text{CHOL}} = \frac{2v_{\text{CHOL}}}{h} \quad (5)$$

3.3.2. Lipid Order Parameter. The average deuterium order parameter $\langle S \rangle$ of both *sn*-1 and *sn*-2 chains of PC in all A–D series as a function of carbon number was calculated using the Gromacs analysis tool *g_order*.³⁸ The average orientational order parameter of CHOL in C and D series was also calculated. This order parameter of CHOL is defined as $\langle (3 \cos^2 \theta - 1)/2 \rangle$ where θ is the angle between the z -axis (the membrane normal) and the plane of the sterol rings as determined by the three carbon atoms C5, C13, and C16 in the united-atom topology of cholesterol.³⁹ The above angular bracket represents the average over all of the lipid molecules involved within a given region, that is, AL or nAL. All lipid order parameters were calculated over the last 25 ns of the simulations.

3.3.3. Transbilayer Density Profile. The transbilayer density profiles for different atom types, the phosphorus of PC (P), the 3- β oxygen of CHOL (C), and the oxygen of water (W), defined as $\rho_P(z)$, $\rho_C(z)$, and $\rho_W(z)$, respectively, were calculated over the last 25 ns of the simulations for both the AL and the nAL regions. The calculation of $\rho_i(z)$ for the i th atom type is given by

$$\rho_i(z) = \frac{N_i(z)}{A \Delta z} \quad i = \text{P, C, or W} \quad (6)$$

Here, $N_i(z)$ is the number of particles for the i th atom type within a thin z -slice at the z -coordinate, A is the area of the AL column or the nAL region, and Δz is the thickness of the z -slice, which also limits the z -resolution of the density calculation. In this study, Δz was fixed at 0.32 nm. The irregular cross-section area A was calculated by a Monte Carlo integration method. See sections S2 and S3 in SI for the details of the calculations of A and $N_i(z)$.

3.3.4. Protein Secondary Structures. The secondary structures of $\text{A}\beta_{40}$ and $\text{A}\beta_{42}$ were analyzed by a defined secondary structure of protein (DSSP) program.^{54,55} Snapshots of proteins with detailed secondary structures obtained from DSSP were generated by the visualization programs, Molscript v2.1⁵⁶ and Raster3D v2.9.2.⁵⁷ Snapshots of protein in the presence of lipid bilayers were generated by the visual molecular dynamics program VMD v1.8.7.⁵⁸

3. RESULTS

3.1. Starting Simulation Structures of $\text{A}\beta$ /Lipid/Water/Ion Complexes. The initial structures of $\text{A}\beta_{40}$ and $\text{A}\beta_{42}$ in this study are illustrated in Figure 1. The atomic coordinates of $\text{A}\beta_{40}$ were obtained from the published solution-structure of $\text{A}\beta_{40}$ in a micelle–water environment, a mimic of the water–lipid bilayer, according to Coles et al.¹¹ To create the initial structure of $\text{A}\beta_{42}$, two residues, ILE and ALA, were added to the C-terminus of $\text{A}\beta_{40}$ (see Materials and Methods section). Both $\text{A}\beta_{40}$ and $\text{A}\beta_{42}$ in this study had a net charge of −3, and the charge distribution among the residues is depicted in Figure 1. In $\text{A}\beta_{40}$, there are six negatively charged residues: Glu-3, Asp-7, Glu-11, Glu-22, Asp-23, and a deprotonated Val-40 (C-terminus), and three positively charged residues: Arg-5, Lys-16, and Lys-28. The charge distribution of $\text{A}\beta_{42}$ differs from that of $\text{A}\beta_{40}$ only in the location of the negatively charged C-terminus, which is at Ala-42.

Both $\text{A}\beta_{40}$ and $\text{A}\beta_{42}$ can be divided into structurally distinct segments: an N-terminal random coil (residues 1–14), a C-terminal α -barrel (residues 15–36), and a short random coil tail (residue 37–40 for $\text{A}\beta_{40}$ and 37–42 for $\text{A}\beta_{42}$). Within the C-terminal region, a transmembrane lipid insertion domain (LID) spans residues 28–40 or 42 for $\text{A}\beta_{40}$ or $\text{A}\beta_{42}$, respectively. The LID is highlighted in Figure 1. Except for the initial positively

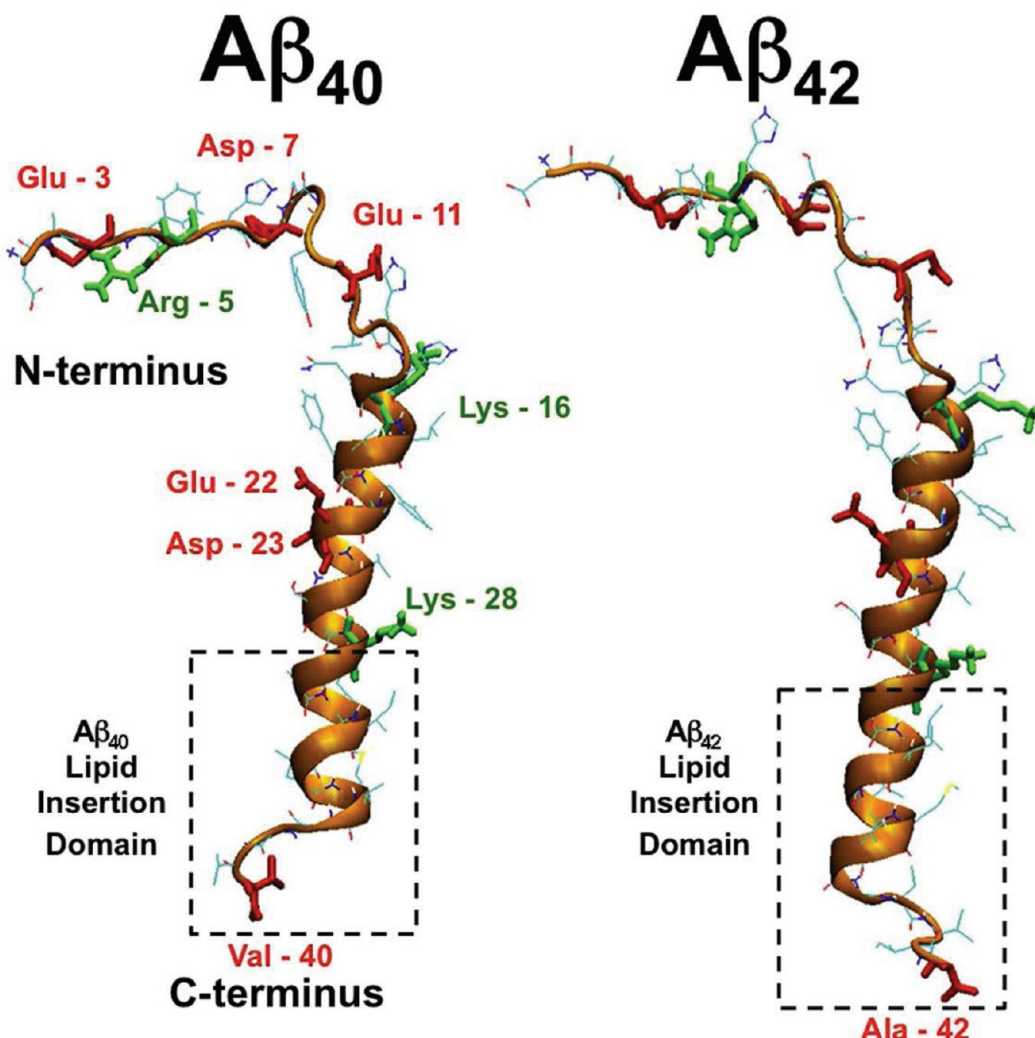


Figure 1. Initial or 0 ns simulated structures of $\text{A}\beta_{40}$ and $\text{A}\beta_{42}$. The initial secondary structure of either $\text{A}\beta_{40}$ or $\text{A}\beta_{42}$ consists of the N-terminal (residue 1 to 14) in a random-coil structure and the C-terminal in an α -helix barrel (residue 15 to 36) and a random coil (residue 37 to 40 or 42). The gold ribbon and line represent the α -helix and random coil structure, respectively, of the backbone of each peptide. The lipid insertion domain, Lys-28 to 40 or Lys-28 to 42 of $\text{A}\beta_{40}$ or $\text{A}\beta_{42}$, respectively, of each peptide is shown inside a dashed-box. Each peptide was partially inserted into the PC or PC/CHOL bilayers with the lipid insertion domain buried into the upper layer of the lipid bilayer with the Lys-28 locating on the phosphate headgroup/water interface. The positively charged residues (Arg-5, Lys-16, and Lys-28) of the protein are in green, whereas the negatively charged residues (Glu-3, Asp-7, Glu-11, Glu-22, Asp-23, and Val-40 or Ala-42) are in red.

charged Lys-28 and the negatively charged C-terminus, the peptides in this short domain are neutral and highly hydrophobic.¹¹

Each $\text{A}\beta$ /lipid/water/ion complex was constructed by inserting $\text{A}\beta_{40}$ or $\text{A}\beta_{42}$ into a PC or PC/CHOL bilayer. Initially, the LID of the protein was placed in the void created at the center of the upper bilayer leaflet. In each case, the C-terminus of the protein was placed at the center of the bilayer ($z = 0$), with the long axis of the α -barrel in a vertical orientation, parallel to the z -axis or the bilayer normal, as demonstrated in Figure 2. This orientation brought the positively charged Lys-28 near the lipid–water interface after the energy minimization and solvation steps (see Materials and Methods section). Note that this partially inserted structure represents a possible membrane location of $\text{A}\beta$ upon its release from the APP by the sequential proteolytic cleavages of β - and γ -secretases *in vivo*.^{3,9,11}

The first column of Figure 2 depicts the initial structures of the four $\text{A}\beta$ /lipid complexes: $\text{A}\beta_{40}$ in PC (A0), $\text{A}\beta_{42}$ in PC (B0),

$\text{A}\beta_{40}$ in PC/CHOL (C0), and $\text{A}\beta_{42}$ in PC/CHOL (D0), where 0 indicates the initial structure. Water molecules were present in all complexes but for clarity are not shown in Figure 2. These four molecular complexes represent $\text{A}\beta$ proteins of two different chain lengths (40 and 42 residues) in two different lipid environments, PC and PC/CHOL. These complexes mimic the $\text{A}\beta$ peptides in the cholesterol-depleted or cholesterol-enriched domains of heterogeneous neuronal membranes immediately after being released from the APP by the secretases.³

3.2. Protein Orientations in Cholesterol-Depleted and Enriched Membranes. Each starting structure, A0, B0, C0, or D0 (first column), underwent four independent 200 ns MD simulations or replicates. The next four columns (2nd to 5th) of Figure 2 display the final 200 ns structures of each replicate. These are identified as A1–A4, B1–B4, C1–C4, and D1–D4, for $\text{A}\beta_{40}$ in PC, $\text{A}\beta_{42}$ in PC, $\text{A}\beta_{40}$ in PC/CHOL, and $\text{A}\beta_{42}$ in PC/CHOL, respectively. Although water molecules were present

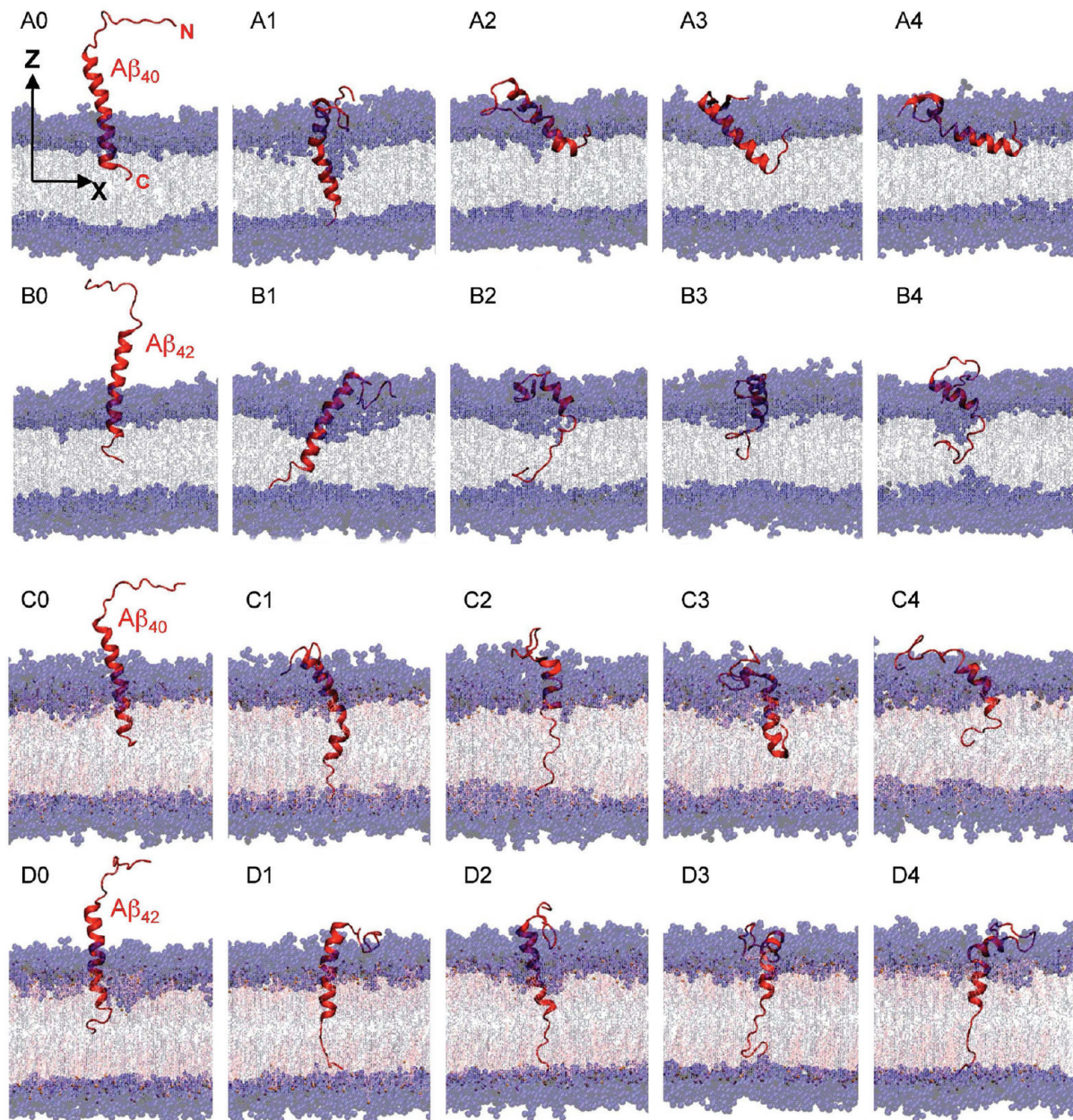


Figure 2. Summary of 200 ns simulated structures of $\text{A}\beta_{40}$ and $\text{A}\beta_{42}$ in cholesterol-depleted and cholesterol-enriched lipid domains. (A1–A4) $\text{A}\beta_{40}$ in PC, (B1–B4) $\text{A}\beta_{42}$ in PC, (C1–C4) $\text{A}\beta_{40}$ in PC/CHOL, and (D1–D4) $\text{A}\beta_{42}$ in PC/CHOL. The initial structures (A0, B0, C0, and D0) of the above are also shown for comparison. For the protein, the red ribbon and line represent the α -helix and random coil structure, respectively, of the backbone of each peptide. For the lipid bilayer, the blue spheres represent the polar groups of PC, gray lines the acyl chains of PC, red sticks the cholesterol, and gold spheres the polar headgroups of cholesterol. The Z-axis indicates the normal of the bilayer. Water was present during the simulations but is not shown for clarity.

during the simulations, they are not shown for clarity in Figure 2. To highlight the hydrophobic region of the bilayer, the acyl chains of PC and the nonpolar region (fused rings and chain) of CHOL are labeled in gray and red, respectively. The polar regions, the polar headgroup of PC, and the 3- β OH headgroup of CHOL are labeled in blue and gold, respectively.

Figure 2 is a molecular-level visualization of the protein insertion efficiency or the probability of insertion in a replicate within the 200 ns observation time of this study. In PC bilayers (A and B series), only A1 for $\text{A}\beta_{40}$ (or 25% of the A-series replicates) and B1 and B2 for $\text{A}\beta_{42}$ (or 50% of the B-series

replicates) exhibited complete insertion into the bilayer: the “fully-inserted” state. Here, the fully inserted state was indicated by the C-terminus of the protein migrating through the acyl chain region and anchoring at the polar PC headgroup region of the lower monolayer. For the case of $\text{A}\beta_{40}$ in PC (A-series), the three other replicates (A2–A4) adopted a membrane surface–interaction state, in which the long axis of the α -barrel within the C-terminal segment tended to align parallel to the x - y plane or the plane of the bilayer. Interestingly, the C-terminus of the A2–A4 replicate protein anchored in the PC polar headgroup region of the upper lipid monolayer instead of the lower lipid monolayer

Table 1. Summary of Secondary Structures of $\text{A}\beta_{40}$ and $\text{A}\beta_{42}$ in PC and PC/CHOL Bilayers

replicate	state	α -helix, ^a non-LID	β -sheet, ^a non-LID	α -helix, ^b LID	β -sheet, ^b LID
$\text{A}\beta_{40}$ in PC					
A0	partially inserted	32.5	0	22.5	0
A1	fully inserted	31.2 \pm 1.7	0 \pm 0	24.8 \pm 0.8	0 \pm 0
A2	surface	32.8 \pm 3.8	0 \pm 0	18.3 \pm 3.1	0 \pm 0
A3	surface	32.1 \pm 0.9	9.3 \pm 5.4	19.3 \pm 2.4	0 \pm 0
A4	surface	31.2 \pm 4.0	9.5 \pm 2.2	19.9 \pm 0.8	0 \pm 0
$\text{A}\beta_{42}$ in PC					
B0	partially inserted	35.7	0	23.8	0
B1	fully inserted	35.2 \pm 1.5	0 \pm 0	21.4 \pm 0.3	0 \pm 0
B2	fully inserted	20.0 \pm 5.9	0 \pm 0	2.2 \pm 3.3	0 \pm 0
B3	partially inserted	32.4 \pm 2.1	0 \pm 0	3.8 \pm 1.9	0 \pm 0
B4	partially inserted	25.2 \pm 4.1	0 \pm 0	4.7 \pm 3.4	0 \pm 0
$\text{A}\beta_{40}$ in PC/CHOL					
C0	partially inserted	32.5	0	22.5	0
C1	fully inserted	37.4 \pm 0.4	0 \pm 0	18.6 \pm 1.8	0.0 \pm 0.3
C2	fully inserted	22.1 \pm 1.7	6.3 \pm 5.1	0.0 \pm 0.1	0.5 \pm 1.4
C3	partially inserted	15.1 \pm 2.9	0 \pm 0	21.1 \pm 2.2	0.2 \pm 1.7
C4	partially inserted	19.1 \pm 5.9	0 \pm 0	12.9 \pm 4.2	0.9 \pm 1.4
$\text{A}\beta_{42}$ in PC/CHOL					
D0	partially inserted	35.7	0	23.8	0
D1	fully inserted	35.7 \pm 0.4	0 \pm 0	14.7 \pm 1.1	0 \pm 0
D2	fully inserted	33.5 \pm 4.6	1.6 \pm 4.0	16.6 \pm 0.5	0 \pm 0
D3	fully inserted	33.4 \pm 5.8	0 \pm 0	5.4 \pm 1.2	0 \pm 0
D4	fully inserted	29.5 \pm 2.1	0.0 \pm 0.3	14.1 \pm 0.7	0 \pm 0

^a Non-LID region (Asp-1 to Asn-27). ^b LID region (Lys-28 to C-terminus). Results (mean \pm SD) from DSSP analysis over the last 25 ns of the 200 ns simulations.

as in A1. This anchoring to the upper monolayer helped stabilize the surface state throughout the 200 ns simulation time. For $\text{A}\beta_{42}$ in PC (B-series), the long axis of the alpha barrel of the protein in B3 was oriented along the membrane normal, whereas that of B4 was tilted. However, the C-terminus of B3 and B4 was not anchored to the headgroups of either leaflet but instead dangled near the middle of the bilayer. Hence, B3 and B4 were designated “partially inserted”.

In PC/CHOL bilayers (C and D series), two replicates of $\text{A}\beta_{40}$ (C1 and C2, 50% of C-series) and all four replicates of $\text{A}\beta_{42}$ (D1–D4, 100% of D-series) ended in the fully inserted state. The other two $\text{A}\beta_{40}$ replicates, C3 and C4, were partially inserted. The above assignments of surface, partially inserted and fully inserted states of all replicates, are summarized in Table 1.

3.3. Protein Conformational Transition in Cholesterol-Depleted and Enriched Membranes. The conformational structures of $\text{A}\beta$ in lipid bilayers were examined by DSSP analysis (see Materials and Methods). A summary of the secondary structures, expressed as the percentage of residues participating in the α -helix and β -sheet structures of the protein, at the beginning and during the last 25 ns of the simulations, is shown in Table 1. Here, we are primarily interested in the conformational transition of two domains, the non-LID (Asp-1 to Asn-27) and the LID (Lys-28 to C-terminus), as described earlier and shown in Figure 1. As noted in Materials and Methods, the LID represents the portion of the peptide that was preinserted into the upper-leaflet of the bilayer in the initial structure. The non-LID region contains the entire random coil N-terminal (residues

1–14) and the first part of the C-terminal (residues 15–27), whereas the LID region covers the rest of the C-terminal.

The conformational transition of $\text{A}\beta$ in PC bilayers (A and B series) is examined first. Figure 3 shows the evolution of the secondary structure of the protein or DSSP profile throughout the entire 200 ns simulations for several replicates, that is, A1, A4, B1, and B2. Here A1, B1, and B2 were in the fully inserted state, whereas A4 was in the surface state. As shown in Figure 3, the α -helix structure of both A1 and B1 was largely preserved in both non-LID and LID regions. In contrast, a significant protein folding from a random coil to a β -sheet structure was found in the N-terminal segment (residue 1–14) of the non-LID region for the surface state, A4. Yet, the α -structure for both non-LID and LID regions of A4 was also preserved. For B2, a moderate unfolding from 35.7–20% in the non-LID, but a large unfolding from 23.8–2.2% in the LID of α -helix was evident as shown in Figure 3 and Table 1. The other replicates in the A-series, A2 and A3, were similar to A4 in α -helix content, but A2 did not show a β -sheet structure as shown in Table 1. The B-series replicates B3 and B4 were in the partially inserted state and showed similar α -helix contents to B1 and B2 and no evidence of β -sheet formation.

The conformational transition of $\text{A}\beta$ in PC/CHOL bilayers (C and D series) was examined next. Figure 4 shows the DSSP profiles for several replicates, that is, C1, C2, D1, and D3, all in the fully inserted state at the end of the simulations. Similar to A1 or B1, the α -helix content of C1, D1, D2, and D4 was largely preserved. In contrast, there was a large unfolding of α -helix from

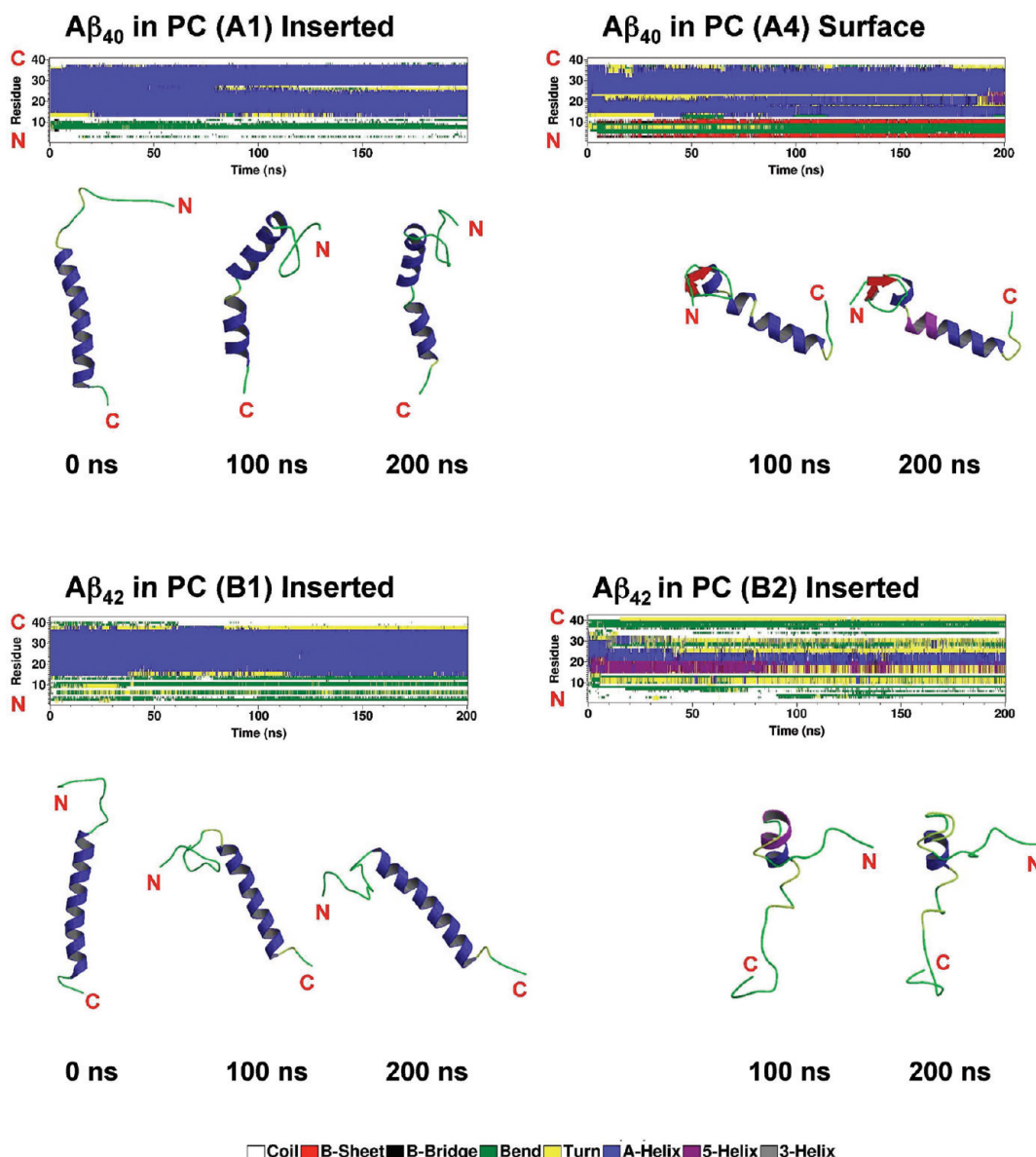


Figure 3. Representative secondary structures as a function of simulation time for $A\beta_{40}$ and $A\beta_{42}$ in cholesterol-depleted lipid domains. The secondary structures of $A\beta_{40}$ and $A\beta_{42}$ in PC bilayers were calculated by DSSP from the representative trajectories, A1, A4, B1, and B2. At the end of the 200 ns simulations, A4 was in the surface state while A1, B1, and B2 were in the fully inserted state (see Figure 2 and Table 1). Snapshot structures of the peptides at some representative simulation time points based on DSSP analysis are also shown. The location of the end C- or N-terminus is indicated for clarity.

22.5 to 0% in C2 and 23.8 to 5.2% in D3. For the other replicates in the C-series, C3 and C4 were in the partially inserted state with about 13–20% α -helix in both non-LID and LID regions as shown in Table 1.

The more detailed atomistic structures of A1, B1, C1, and D1, all fully inserted states, are shown in Figure 5. It is clear that the LID of either $A\beta_{40}$ or $A\beta_{42}$ was completely embedded into the acyl chain region, while the non-LID stayed mainly within the polar region of the bilayer. The positively charged Lys-28 and negatively charged C-terminus, marking the beginning and end residues of the LID region as shown in Figure 1, respectively, were found to attach to the negatively charged nitrogen (N4) of PC of the upper layer and the positively charged phosphorus (P8) of PC of the lower layer, respectively.

3.4. Protein-Induced Membrane Disruption in Cholesterol-Depleted and Enriched Membranes. The extent of membrane disruption by $A\beta_{40}$ or $A\beta_{42}$ in different states (surface and inserted) in PC and PC/CHOL was studied. The membrane disruption was quantified by three biophysical parameters: surface area per lipid (Figure 6), transbilayer density thickness of lipid polar group and water (Figure 7), and order parameter of lipid (Figures 8–10). These parameters were determined for both the annular lipids (ALs) and the nonannular lipids (nALs), as described in Materials and Methods. The differences in membrane parameters between the ALs and nALs provide sensitive, noninvasive indicators of protein-induced membrane disruption in cholesterol-depleted and enriched membranes. As important controls for assessing the protein effects on the

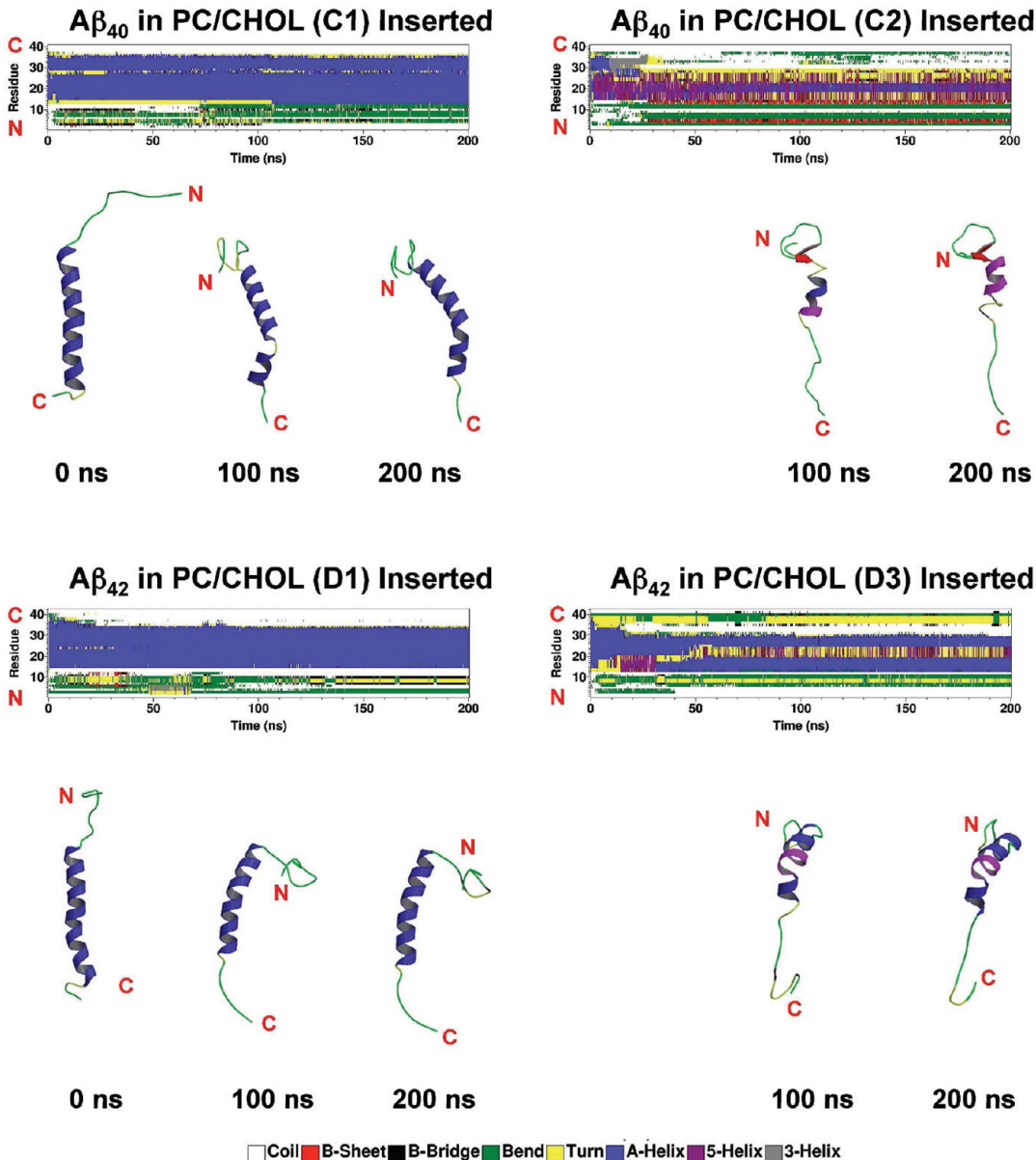


Figure 4. Representative secondary structures as a function of simulation time for $\text{A}\beta_{40}$ and $\text{A}\beta_{42}$ in cholesterol-enriched lipid domains. The secondary structures of $\text{A}\beta_{40}$ and $\text{A}\beta_{42}$ in PC/CHOL bilayers were calculated by DSSP from the representative trajectories, C1, C2, D1, and D3. At the end of the 200 ns simulations, all of the shown trajectories are in the fully inserted state (see Figure 2 and Table 1). See the legend of Figure 3 for more details.

membranes, the above biophysical parameters were also calculated for the pure PC and PC/CHOL bilayers in the absence of protein (see Materials and Methods). The following four subsections describe the results.

3.4.1. Surface Area per Lipid. The average surface area of PC (A_{PC}) was calculated for nALs and ALs for the PC and PC/CHOL bilayers and for the PC lipids in the control pure PC and PC/CHOL bilayers. The last 25 ns of the simulations were used, and the results are summarized in Figure 6. In the PC membrane, the A_{PC} of the nALs was 66.24 \AA^2 for the surface state of $\text{A}\beta_{40}$ and 63.14 \AA^2 for the inserted state of $\text{A}\beta_{42}$ but increased to 73.87 and 68.05 \AA^2 for the ALs, representing a change of ~ 12 and 8% , respectively. The A_{PC} in the control, that is, pure PC without protein, was 65.50 \AA^2 , very similar to the calculated value of A_{PC} of the nALs. In the PC/CHOL membrane, the A_{PC} of the nALs was 52.54 \AA^2 for $\text{A}\beta_{40}$ and 50.92 \AA^2 for $\text{A}\beta_{42}$, all in the inserted

state. These values increased to 70.52 and 65.21 \AA^2 for the ALs, respectively, that amounted to an increase of ~ 34 and 28% , respectively. The A_{PC} of the pure PC/CHOL bilayers (control) was 51.15 \AA^2 , similar to the A_{PC} of the nALs noted above.

The average surface area of CHOL (A_{C}) was also calculated for both nALs and ALs in the PC/CHOL bilayers as well as for all the cholesterol in the control pure PC and PC/CHOL bilayers over the last 25 ns of the simulations, and the results are summarized in Figure 6. The A_{C} of the nALs was 31.75 \AA^2 for $\text{A}\beta_{40}$ and 30.81 \AA^2 for $\text{A}\beta_{42}$ and was 30.05 and 29.75 \AA^2 for the ALs, respectively. The A_{C} of the pure PC/CHOL (control) was 31.15 \AA^2 , very close to the values in ALs or nALs described above.

3.4.2. Transbilayer Density Profiles of Lipid Polar Group and Water. The transbilayer, or z-dependent, number density profiles of PC polar headgroup phosphorus (P8), cholesterol 3- β hydroxyl oxygen (O6) and water oxygen were calculated for all the A-D

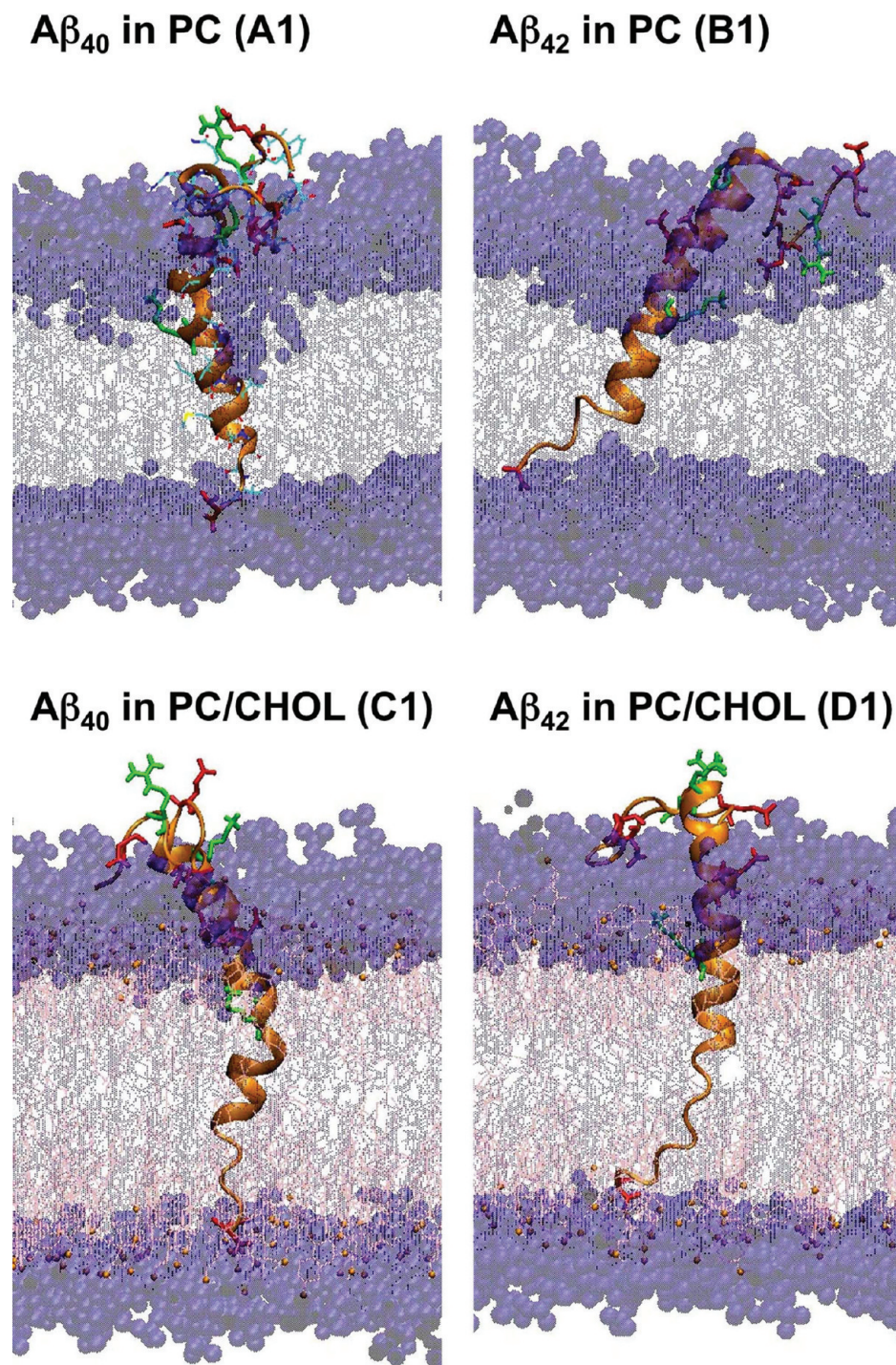


Figure 5. Representative 200 ns simulated fully inserted structures of $\text{A}\beta_{40}$ and $\text{A}\beta_{42}$ in cholesterol-depleted and enriched lipid domains. The representative secondary structures of $\text{A}\beta_{40}$ in PC (A1), $\text{A}\beta_{42}$ (B1), $\text{A}\beta_{40}$ in PC/CHOL (C1), and $\text{A}\beta_{42}$ in PC/CHOL (D1), all in the fully inserted state, are shown. See the legends of Figures 1 and 2 for details.

series and the control PC and PC/CHOL bilayers. These computations used data from the last 25 ns of the simulations (see Materials and Methods). Here z is defined as the normal of the bilayers with $z = 0$ at the mid plane of the bilayer. Representative profiles of the A and B series are shown in Figures S2A and S2B and those of the C and D series in Figures S3A and S3B in SI. Two well-defined phosphorus peaks characterize the

PC phosphate headgroup distributions in the lower (negative z) and upper (positive z) leaflets of both PC and PC/CHOL bilayers. Similarly, cholesterol polar oxygen peaks in the upper and lower leaflets indicate the cholesterol polar headgroup distributions. The peak-to-peak PC-phosphorus and CHOL-oxygen z -distances, z_P and z_C , respectively, provide a measure of the average transbilayer thickness of PC and CHOL in the lipid bilayer.

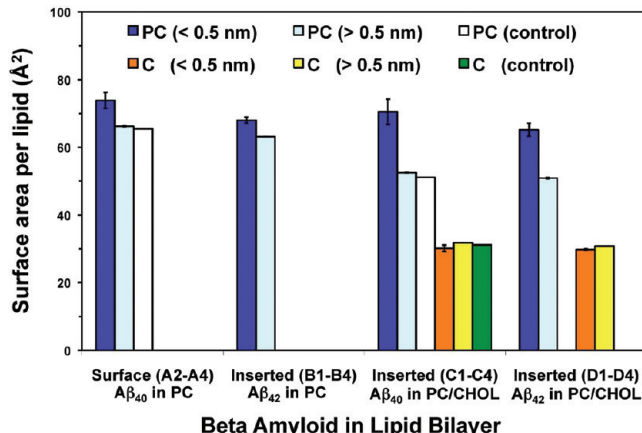


Figure 6. Summary of the surface area per lipid of PC and cholesterol for $\text{A}\beta_{40}$ and $\text{A}\beta_{42}$ in cholesterol-depleted and cholesterol-enriched lipid domains. The calculated surface area of PC and CHOL of the ALs (dark blue and orange, respectively) and of the nALs (light blue and yellow, respectively) in the PC or PC/CHOL. The surface area per lipid was also calculated in pure PC (white) and PC/CHOL (green) bilayers in the absence of $\text{A}\beta$ peptide. The surface area was calculated over the last 25 ns of the 200 ns simulations. The error bar represents the SE ($= \text{SD}/N^{1/2}$, where $N = \text{number of replicates}$) of the mean.

The number density of water oxygen decreased progressively as the relative z -distance from the bilayer center, or $|z|$, decreased in the upper and lower layers as shown in Figures S2A, S2B, S3A, and S3B of the SI. Therefore, this z -profile of water density provides useful information about the transbilayer water permeability barrier of the lipid bilayer. To provide a quantitative measure of this permeability barrier, the z -distance of the water density profile at a fixed density of 1 nm^{-3} , defined in here as the “critical” transbilayer water barrier or z_w , was determined. The critical density of 1 nm^{-3} is $\sim 3\%$ of the known number density of bulk water, which is about 33.3 nm^{-3} . This 1 nm^{-3} critical density provided a common gauge to compare water barrier thickness among the bilayer membranes of all six series, that is, A–D and two pure bilayer controls.

The above three transbilayer membrane parameters (z_p , z_c , and z_w) calculated from the density profiles of the ALs and nALs of all replicates in series A–D and in the two bilayer controls over the last 25 ns of the simulations are summarized in Figure 7. Similar to those of surface area in Figure 6, the data shown in Figure 7 represent averages over the combined partially and fully inserted states for either $\text{A}\beta_{42}$ in PC (B1–B4) or $\text{A}\beta_{40}$ in PC/CHOL (C1–C4).

The results of the transbilayer PC thickness were first examined. In the nALs of the PC bilayers (Figure 7), the average z_p was 3.50 nm for the surface state of $\text{A}\beta_{40}$ and 3.66 nm for the inserted state of $\text{A}\beta_{40}$. However, these values dropped to 3.24 and 3.07 nm in the ALs, a decline of ~ 7 and 16%, respectively. For comparison, the z_p was 3.62 nm in pure PC bilayers (control) and very similar to the above values in the nALs. The nALs of PC/CHOL bilayers showed an average z_p of 4.16 nm for $\text{A}\beta_{40}$ and 4.29 nm for $\text{A}\beta_{42}$ both in the inserted state. Yet z_p for the ALs was 3.67 and 3.83 nm, ~ 12 and 11% less than the nALs. Also for comparison, the z_p was 4.25 nm in pure PC/CHOL bilayers (control) and very similar to the above values in the nALs. We notice that the overall z_p of the pure PC/CHOL bilayers was $\sim 17\%$ larger than that of the pure PC bilayers. This

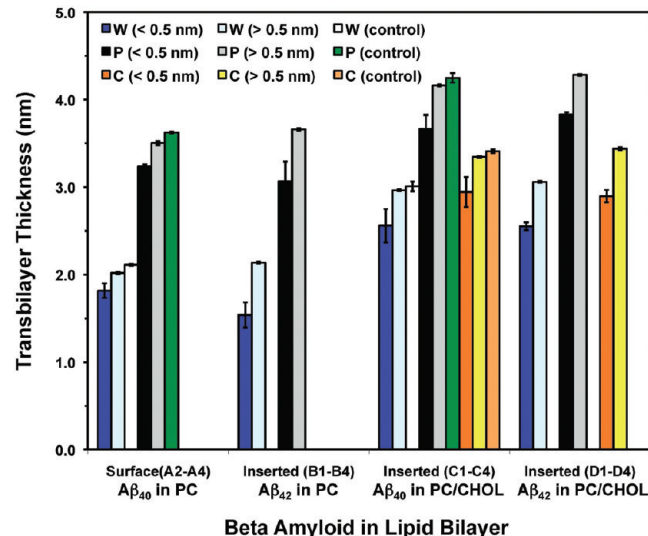


Figure 7. Summary of the transbilayer thickness of PC and cholesterol polar groups and critical water thickness for $\text{A}\beta_{40}$ and $\text{A}\beta_{42}$ in cholesterol-depleted and cholesterol-enriched lipid domains. The transbilayer thicknesses of the PC and cholesterol headgroup in the AL column, labeled as black and orange, respectively, and in the nAL region, labeled as gray and yellow, respectively, were calculated from the averaged transbilayer peak-to-peak distance of the number density profiles of PC headgroup phosphorus and 3- β hydroxyl polar oxygen in cholesterol, respectively, as demonstrated in Figures S2 and S3 in the SI. For the case of water, the critical thickness was evaluated from the averaged $|z|$ distance of water profile at a fixed number density of 1 nm^{-3} in the ALs (dark blue) and in the nALs (light blue) also demonstrated in Figures S2 and S3 in SI. The plot represents the average of all three surface states (A2–A4 for $\text{A}\beta_{40}$ in PC), combined partially and fully inserted states (B1–B4 for $\text{A}\beta_{42}$ in PC and C1–C4 for $\text{A}\beta_{40}$ in PC/CHOL) and all fully inserted states (D1–D4 for $\text{A}\beta_{42}$ in PC/CHOL). The above thickness parameters of PC, cholesterol, and water were also calculated in pure PC and PC/CHOL bilayers in the absence of $\text{A}\beta$ peptide and are labeled in white, green, and orange bars, respectively. All calculations were performed over the last 25 ns of the 200 ns simulations. The error bar represents the SE of the mean.

cholesterol-induced increase in bilayer thickness is clearly evident in Figures 2 and 5.

The results of the transbilayer cholesterol thickness in PC/CHOL were also examined. Here the average z_c was 3.35 nm for $\text{A}\beta_{40}$ and 3.44 nm for $\text{A}\beta_{42}$ for the nALs but declined ~ 13 and 15% to 2.94 and 2.90 nm for the ALs. For comparison, the z_c was 3.41 nm in pure PC/CHOL bilayers (control) and very similar to the above values in the nALs.

Overall, the above transbilayer lipid (PC and CHOL) thickness results indicate that the protein created a moderate decline in the bilayer thickness and that in the absence of cholesterol the inserted state protein perturbed the bilayer thickness slightly more than the surface state protein.

Finally, the transbilayer water profile was examined. In the nAL region of PC bilayers, the average z_w was 2.02 nm for the surface state of $\text{A}\beta_{40}$ and 2.13 nm for the inserted state of $\text{A}\beta_{42}$ as shown in Figure 7. However, in the ALs, z_w dropped to 1.82 and 1.54 nm, representing a decline of ~ 10 and 28%, respectively. In the nALs of PC/CHOL bilayers, the average z_w was 2.97 nm for $\text{A}\beta_{40}$ and 3.08 nm for $\text{A}\beta_{42}$ in the inserted state. In the ALs, these values dropped to 2.56 and 2.55 nm, that is, a decline of ~ 14 and 17%, respectively. For comparison, the z_w was 2.11 nm in pure

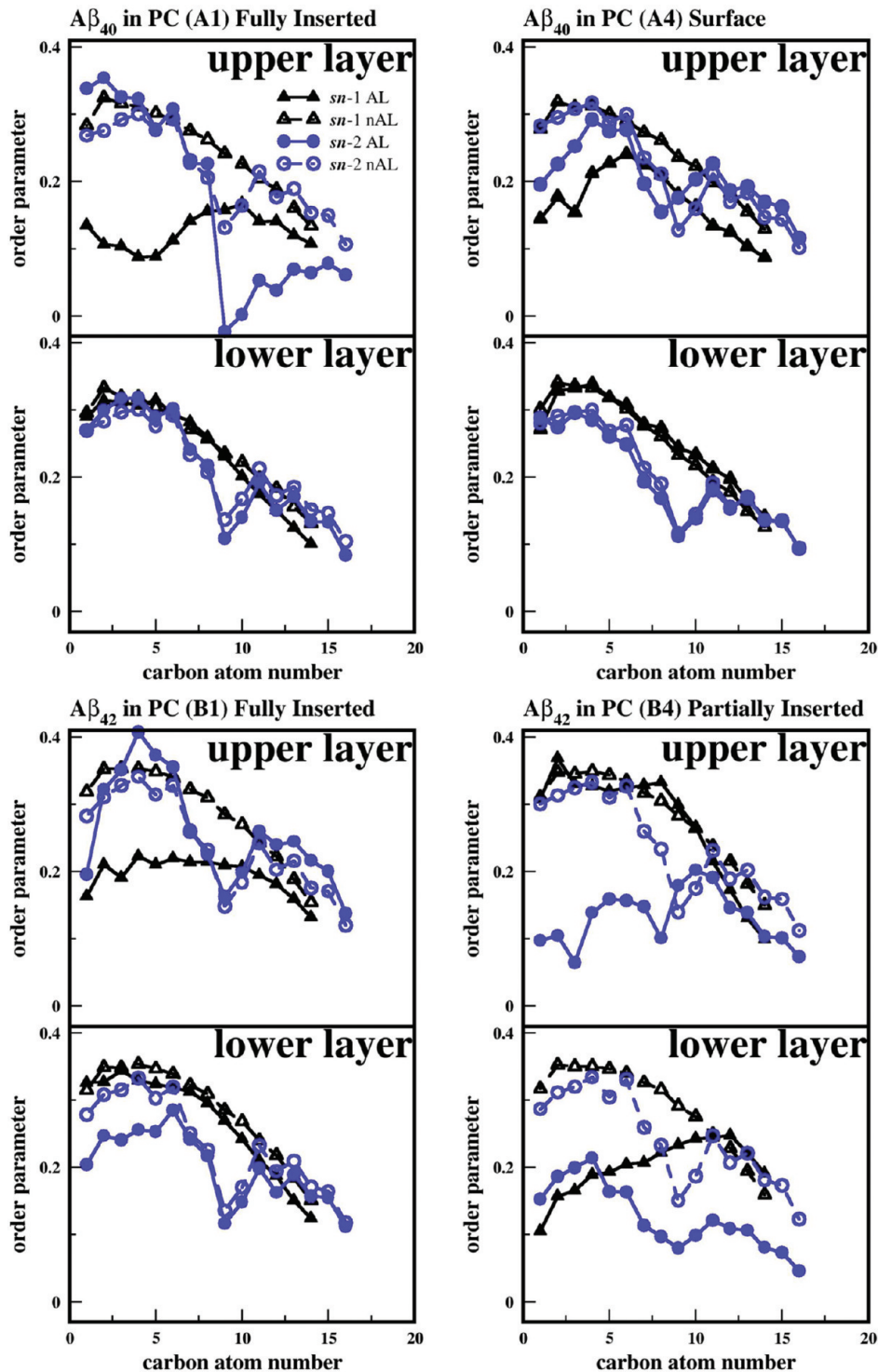


Figure 8. Representative order parameters of PC acyl chains for $A\beta_{40}$ and $A\beta_{42}$ in cholesterol-depleted lipid domains: averaged deuterium order parameters of the *sn*-1 chains of ALs (black solid triangle), the *sn*-1 chains of the nALs (black open triangle), the *sn*-2 chains of ALs (blue solid circle), and the *sn*-2 chains of nALs (blue open circle) in the upper layer ($z > 0$) and the lower layer ($z < 0$) as a function of the carbon number position of the PC acyl chain. The representative plots correspond to the fully inserted states of $A\beta_{40}$ in PC (A1) and $A\beta_{42}$ in PC (B1) and the surface state of $A\beta_{40}$ in PC (A4) and partially inserted state of $A\beta_{42}$ in PC (B4). The order parameters were calculated over the last 25 ns of the 200 ns simulations.

PC and 3.01 nm in pure PC/CHOL, similar to the corresponding value in nALs shown above. These results suggest that the protein induced a larger decline in the water barrier thickness for $A\beta_{42}$ than for $A\beta_{40}$ in either PC or PC/CHOL bilayers. The

observed change was less in PC/CHOL than PC in the inserted state.

3.4.3. Order Parameters of PC Acyl Chains. The average order parameters of the PC acyl chains, *sn*-1 (S_{P1}) and *sn*-2 (S_{P2}), in PC

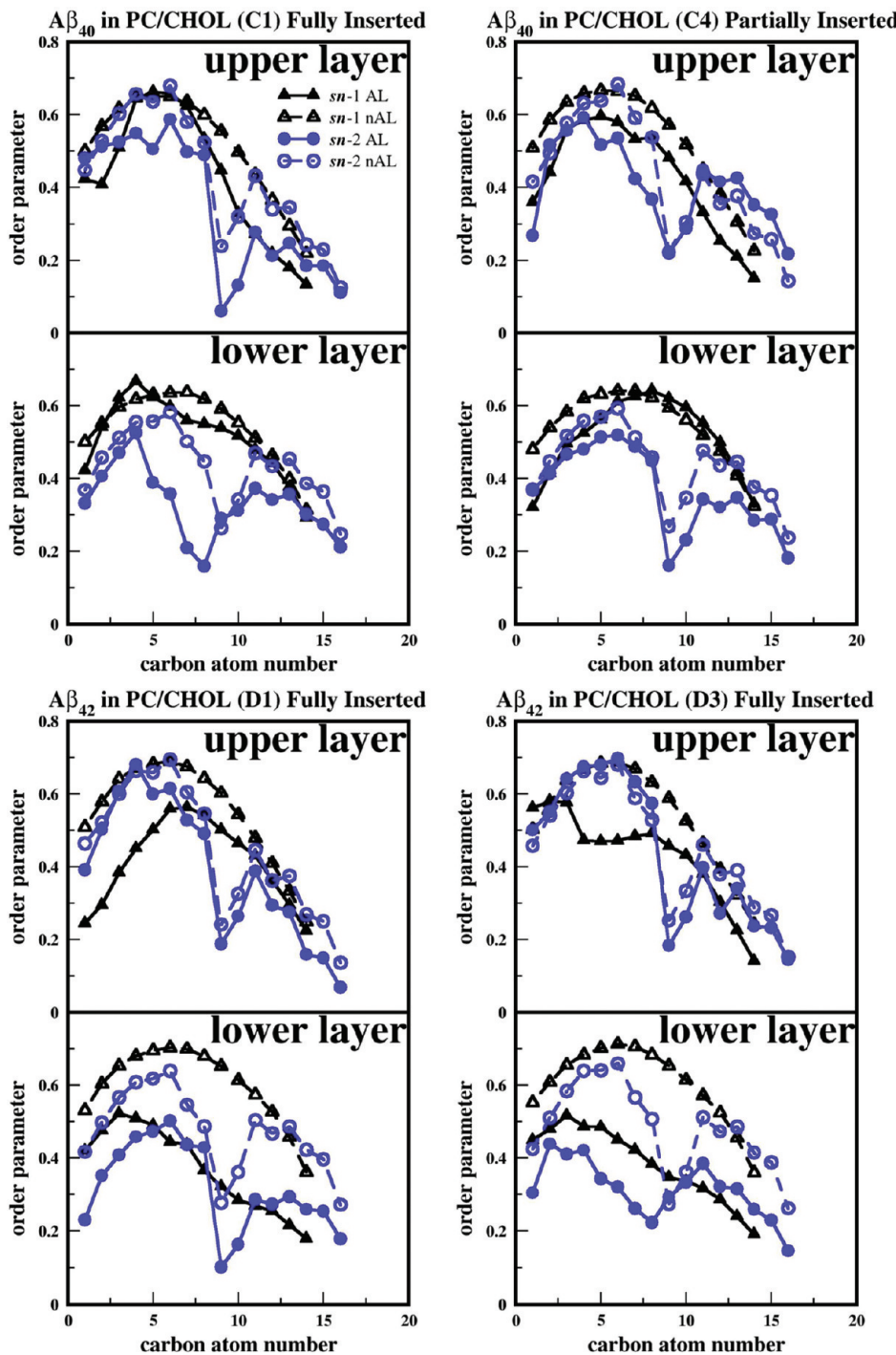


Figure 9. Representative order parameter of PC acyl chains for $\text{A}\beta_{40}$ and $\text{A}\beta_{42}$ in cholesterol-enriched lipid domains: averaged deuterium order parameters of the *sn*-1 chains of ALs (black solid triangle), the *sn*-1 chains of nALs (black open triangle), the *sn*-2 chains of the ALs (blue solid circle), and the *sn*-2 chains of nALs (blue open circle) in the upper layer ($z > 0$) and the lower layer ($z < 0$) as a function of the carbon number position of the PC acyl chain. The representative plots correspond to the fully inserted states of $\text{A}\beta_{40}$ in PC/CHOL (C1), $\text{A}\beta_{42}$ in PC/CHOL (D1 and D3), and partially inserted state of $\text{A}\beta_{40}$ in PC/CHOL (C4). The order parameters were calculated over the last 25 ns of the 200 ns simulations.

bilayers for typical replicates are shown in Figure 8. The results are categorized by proximity to the protein (nALs or ALs) and by leaflet (upper or lower layer). In general, the value of $S_{\text{P}1}$ or $S_{\text{P}2}$ was smaller in the ALs than in the nALs suggesting that the protein disturbed the order of nearby acyl chains. Similar results were seen for PC/CHOL bilayers as demonstrated by Figure 9.

For both $\text{A}\beta_{40}$ and $\text{A}\beta_{42}$ in PC bilayers as illustrated in Figure 8, nALs show a progressive decline in the order parameter of the saturated *sn*-1 chain (16:0) as a function of carbon number (n), and a prominent dip of the order at $n = 9$, the location of the double-bond of the unsaturated *sn*-2 chain (18:1).

For $\text{A}\beta_{40}$ in the fully inserted state (A1), $S_{\text{P}1}$ for $n < 9$ and $S_{\text{P}2}$ for $n > 9$ were much smaller in the ALs than in the nALs of the

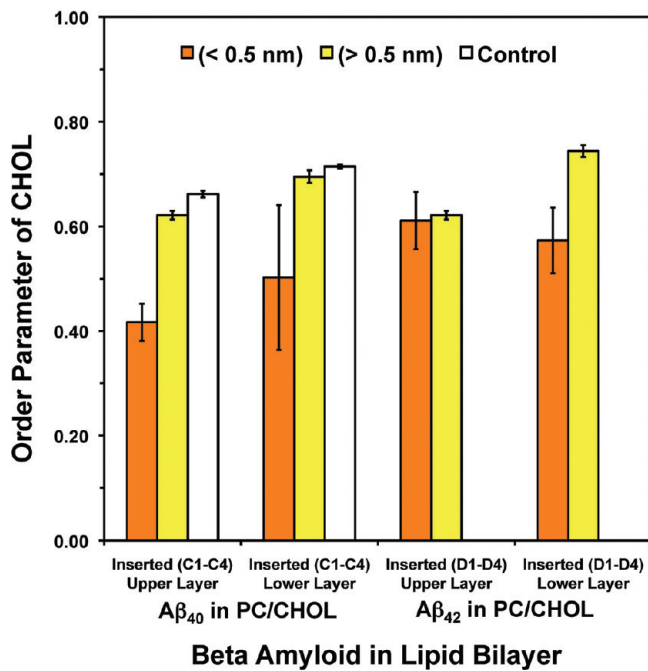


Figure 10. Summary of the cholesterol order parameter for $\text{A}\beta_{40}$ and $\text{A}\beta_{42}$ in cholesterol-enriched lipid domains: averaged order parameter of cholesterol of ALs (orange) and nALs (yellow) in the upper layer ($z > 0$) and the lower layer ($z < 0$) of $\text{A}\beta_{40}$ and $\text{A}\beta_{42}$ in PC/CHOL. The order parameter in pure PC/CHOL in the absence of $\text{A}\beta$ peptide (white) was also calculated. All order parameters were calculated over the last 25 ns of the 200 ns simulations. The error bar represents the SE of the mean.

upper layer. In contrast, for $\text{A}\beta_{40}$ in the surface state (A4), both $S_{\text{P}1}$ and $S_{\text{P}2}$ for $n < 6$ were only slightly smaller in the ALs than in the nALs of the upper layer. These observations indicate that $\text{A}\beta_{40}$ perturbs the acyl chains of the upper layer more effectively when fully inserted than when remaining in the surface state. For the lipids in the lower layer of either A1 or A4, the values of $S_{\text{P}1}$ in the ALs were similar to those in the nALs for all n 's. A similar observation was found for the values of $S_{\text{P}2}$. These results suggest a lack of perturbation of the acyl chain order in the lower layer by $\text{A}\beta_{40}$ in either the inserted or surface state.

For $\text{A}\beta_{42}$ in the fully inserted state (B1), $S_{\text{P}1}$ for $n < 9$ was smaller in the ALs than in the nALs of the upper layer, while $S_{\text{P}2}$ remained the same in ALs and nALs. Again, for the lipids in the lower layer, the values of $S_{\text{P}1}$ or $S_{\text{P}2}$ in ALs were similar to those in the nALs indicating no significant acyl chain perturbation induced by the inserted $\text{A}\beta_{42}$ in the lower lipid layer. For $\text{A}\beta_{42}$ in the partially inserted state (B4), $S_{\text{P}1}$ for all n in ALs was similar to that in nALs, but $S_{\text{P}2}$ for all $n < 9$ was much smaller in the ALs than in the nALs in the upper layer. For the lower layer, $S_{\text{P}1}$ for $n < 9$ and $S_{\text{P}2}$ for all n were much smaller in ALs than in nALs. It is interesting that in the fully inserted state $\text{A}\beta_{42}$ had little effect on the lipid order in the lower lipid layer, but when partially inserted, a large decline for B4 was detected. This suggests that, for pure PC membranes, the partially inserted state is the most perturbing, and that the *sn*-2 chains were preferentially disturbed by $\text{A}\beta_{42}$.

As shown in Figure 9, the values of $S_{\text{P}1}$ and $S_{\text{P}2}$ for lipids in PC/CHOL bilayers were significantly higher than those in the PC bilayers. Here, the fully inserted (C1) or partially inserted (C4) $\text{A}\beta_{40}$ in PC/CHOL bilayers has only moderate perturbation

effects in lowering the $S_{\text{P}1}$ or $S_{\text{P}2}$ of the ALs in the upper layer when compared with the inserted $\text{A}\beta_{40}$ in PC bilayers (see Figure 8). However, for the lower lipid layer, strong perturbations by the inserted or partially inserted $\text{A}\beta_{40}$ in the ALs of PC/CHOL bilayers (Figure 9) were evident when compared with no perturbation at all for the inserted $\text{A}\beta_{40}$ in PC bilayers (see Figure 8). In addition, $\text{A}\beta_{42}$ appeared to be more effective than $\text{A}\beta_{40}$ in inducing acyl chain disorder, especially in the lower leaflet as clearly demonstrated in Figure 9.

As controls, the average $S_{\text{P}1}$ and $S_{\text{P}2}$ of all PC lipids in the pure PC and PC/CHOL bilayers in the absence of protein were calculated over the last 25 ns of the simulations. The results of the controls were directly compared with the order parameters in the nALs for the same representative replicates (A1, A4, B1, B4, C1, C4, D1, and D3) as described above. As demonstrated in Figures S4A and S4B of the SI, the values of $S_{\text{P}2}$ in the upper or lower layer of PC and PC/CHOL were almost identical to those in the nALs of the same bilayers for either $\text{A}\beta_{40}$ or $\text{A}\beta_{42}$. On the other hand, the values of $S_{\text{P}1}$ in the nALs of $\text{A}\beta_{40}$ in PC (A1 and A4) and in PC/CHOL (C1 and C4) bilayers were slightly lower than those in the pure PC. The reverse, that is, the order in control slightly higher than that in nALs, was evident for $\text{A}\beta_{42}$ in PC (B1 and B4) and in PC/CHOL (D1 and D3) bilayers. The difference between the control and the nALs was however much smaller than the large perturbation effect of protein in the ALs as shown in Figures 8 and 9.

3.4.4. Order Parameters of Cholesterol. The cholesterol order parameter (S_{C}) provides a unique measure of the orientational distribution of the long axis of the cholesterol rings with respect to the normal of the PC/CHOL bilayer. Figure 10 summarizes the average S_{C} of ALs and nALs in both upper and lower leaflets of PC/CHOL for $\text{A}\beta_{40}$ and $\text{A}\beta_{42}$. The average S_{C} of nALs was 0.62 in the upper layer and 0.70 in the lower layer for $\text{A}\beta_{40}$, but slightly higher at 0.66 and 0.74, respectively, for $\text{A}\beta_{42}$. Similar to the trend of $S_{\text{P}1}$ and $S_{\text{P}2}$ of PC, the S_{C} of ALs in either upper or lower layer was smaller than that of nALs for both $\text{A}\beta_{40}$ and $\text{A}\beta_{42}$. For the ALs in $\text{A}\beta_{40}$, the average S_{C} was 0.42 in the upper layer and 0.50 in the lower layer, reductions of approximately 32% and 29% compared with that of nALs. For $\text{A}\beta_{42}$, the order parameter declined 8% and 23% between AL and nAL cholesterol for the upper and lower leaflets. Therefore, $\text{A}\beta_{40}$ disrupted the cholesterol orientational distribution in the upper layer more than $\text{A}\beta_{42}$, whereas the extent of disruption was similar in the lower layer. As controls, the average S_{C} of cholesterol was 0.66 in the upper layer and 0.71 in the lower layer of the pure PC/CHOL bilayers. These values were very similar to those in the nALs of the upper and lower layers as described above.

3.4.5. Site-Specific Cholesterol Interaction Dynamics with Protein. Residue-specific cholesterol/protein interaction dynamics based on the time evolution of the minimum distance between the cholesterol and each individual protein residue was examined. Figures 11 and 12 show the kinetics of representative replicates (C1, C2, D1, and D3). Since a cutoff of 5 Å was used to define the AL boundary and a distance range of 0–5 Å was used in generating the plots, Figures 11 and 12 highlight the interaction dynamics of cholesterol within the ALs. It is clear that most of interactions between cholesterol and the protein were within the LID of either $\text{A}\beta_{40}$ or $\text{A}\beta_{42}$. Generally, a large fluctuation in the minimum distance with an average >3 Å was found. However, Lys-28 of C1 (Figure 11) clearly shows a minimum distance of around ~ 2 Å, which remained stable for the last 25 ns of the simulations. A previous study of cholesterol interaction dynamics

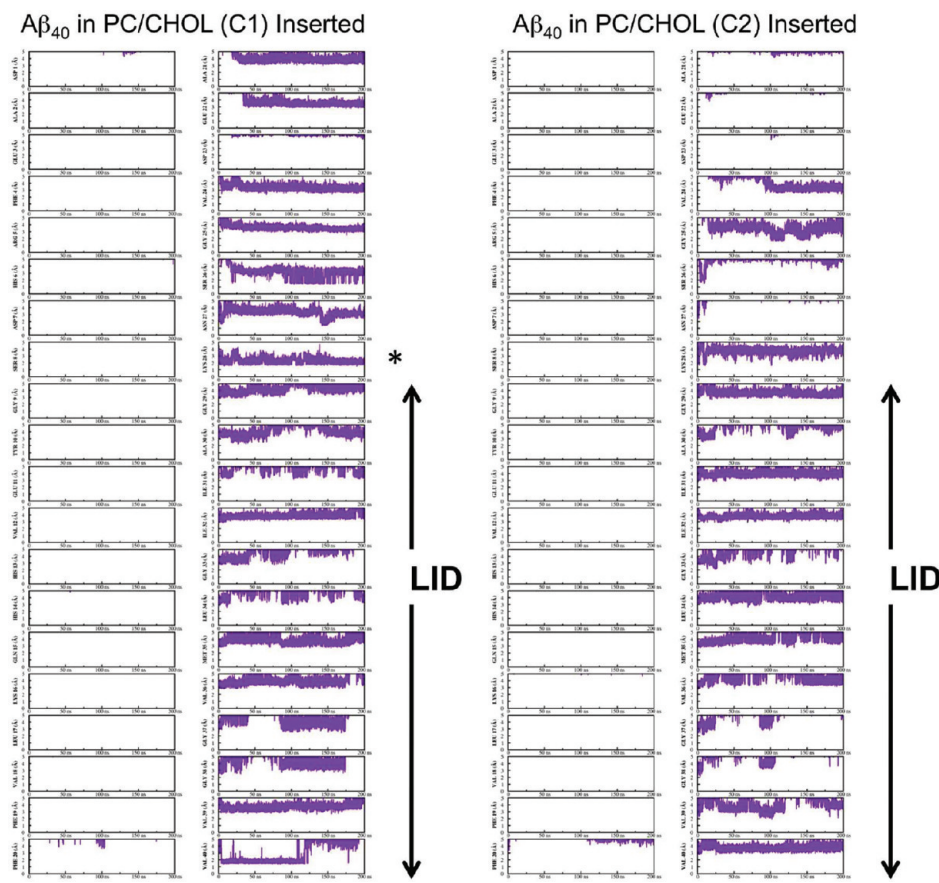


Figure 11. Cholesterol interaction dynamics with $\text{A}\beta_{40}$ in cholesterol-enriched lipid domains. The time evolution of the minimum distance (in Å) between cholesterol and each residue of $\text{A}\beta_{40}$ as a function of simulation time (in ns) is shown. The order of residues starts from the top (N-terminus) to the bottom of the left column and continues with the top to the bottom (residue C-terminus) of the right column. The vertical arrow marks those residues within the LID of each protein. The panel marked with an asterisk indicates the interaction dynamics of cholesterol with Lys-28 where the minimum distance between them was observed to be the shortest ($\sim 2 \text{ \AA}$) and stable when compared with other kinetics plots in the last 25 ns.

with a 17-residue long membrane-active peptide dynorphin A also showed a close interaction distance between cholesterol and Lys-11 of $\sim 2 \text{ \AA}$.¹⁷ A close examination of replicate C1 during the last 25 ns revealed interactions between the 3- β hydroxyl group of cholesterol and the Lys-28 residue of $\text{A}\beta_{40}$ as shown in Figure 13.

To further examine the possibility of local cholesterol enrichment around the protein in the ALs, the local molar ratio of cholesterol X_{CHOL} defined as Chol/(PC + CHOL), was calculated using the last 25 ns of the simulations. For the representative replicates, the value of X_{CHOL} (mean \pm SD of mean) in the ALs was 0.436 ± 0.023 for C1, 0.413 ± 0.030 for C2, 0.369 ± 0.020 for D1, and 0.360 ± 0.026 for D3. For comparison, the value of X_{CHOL} in the nALs was 0.399 ± 0.001 , 0.4000 ± 0.001 , 0.401 ± 0.001 , and 0.402 ± 0.001 , as expected. Hence, no significant enrichment of cholesterol in the ALs, except perhaps a slight increase for C1, was evident. The time evolution of X_{CHOL} in both ALs and nALs for the above replicates are given in Figure S5 of the SI.

4. DISCUSSION

An atomistic MD simulation was employed to examine the role of cholesterol in modulating the membrane interactions of two $\text{A}\beta$ peptides. The peptides, $\text{A}\beta_{40}$ and $\text{A}\beta_{42}$, interacted with

PC and PC/CHOL bilayers that mimic cholesterol-depleted and enriched membrane domains of the neuronal membranes. Starting from a partially inserted membrane orientation, we have used 200 ns simulations to investigate (1) the protein orientation in the lipid bilayer, (2) the protein folding/unfolding behavior in the LID and non-LID regions, and (3) the protein-induced membrane disruption in the bilayers. These three membrane-associated events relate to early membrane interactions of the $\text{A}\beta$ peptide as it is released from the parent-APP by the secretases *in vivo*.³ Sixteen independent simulation replicates and eight pure lipid bilayer controls representing a total simulation time of $4.8 \mu\text{s}$ were successfully generated and systematically analyzed to reveal the role of cholesterol in these membrane interaction events.

The membrane orientation and interaction events of $\text{A}\beta$ with neuronal membranes in atomistic details and biologically relevant time scale are important unsolved problems. This MD simulation study provides evidence that the shorter $\text{A}\beta_{40}$ prefers the surface state over the inserted state in cholesterol-depleted membranes. However, in cholesterol-enriched membranes, the $\text{A}\beta_{40}$ exhibited only partially or fully inserted state with no sign of surface state. For the case of the longer $\text{A}\beta_{42}$, the peptide exhibited only the partially or fully inserted state in cholesterol-depleted membranes but exclusively the fully inserted state in cholesterol-enriched membranes. The unique surface state

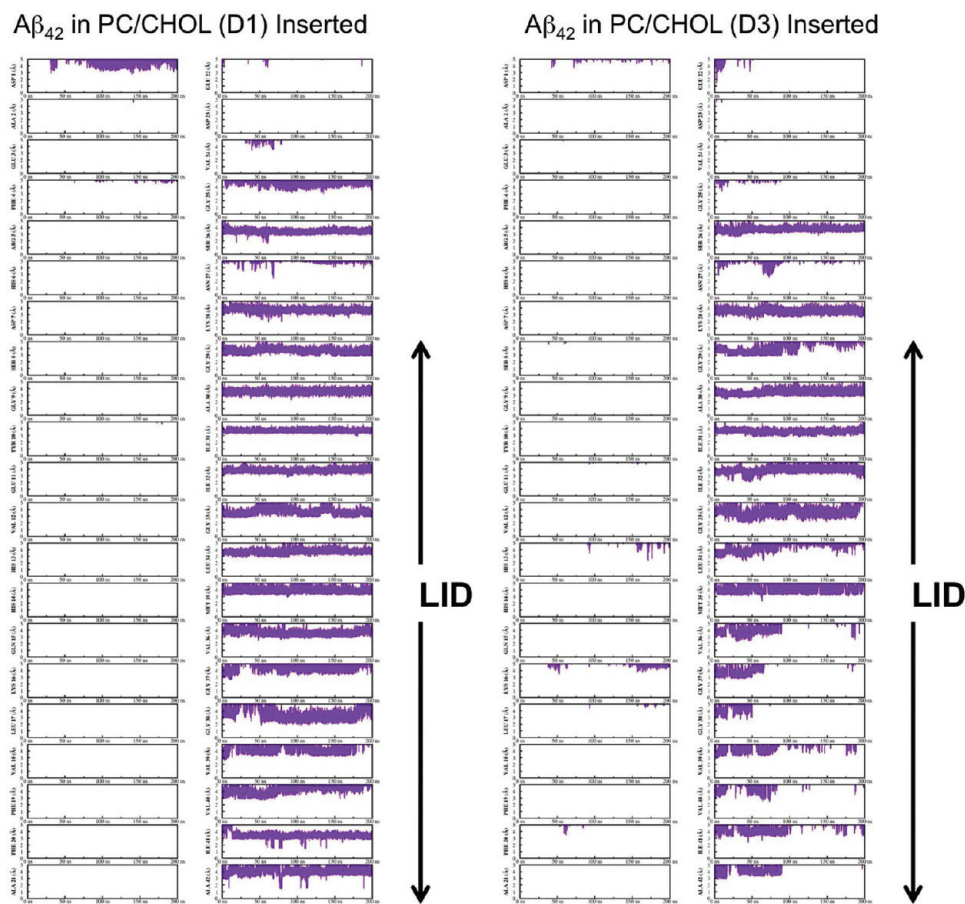


Figure 12. Cholesterol interaction dynamics with $\text{A}\beta_{42}$ in cholesterol-enriched lipid domains. The time evolution of the minimum distance (in Å) between cholesterol and each residue of $\text{A}\beta_{42}$ as a function of simulation time (in ns) is shown. See the legend of Figure 11 for details.

preference of A β ₄₀ in cholesterol-depleted membranes suggests that the shorter A β ₄₀ released in a disordered cholesterol-free lipid domain is likely to migrate to the membrane surface. On the other hand, in a more ordered lipid domain with cholesterol, or a lipid raft, newly released A β ₄₀ will stay in the inserted orientation. For the more hydrophobic, longer A β ₄₂, the peptide stays in the inserted orientation whether or not it is released in a cholesterol-enriched domain. However, the depth and possibly the stability of the inserted state do depend on cholesterol enrichment. These observations indicate the importance of the site of A β release in the highly heterogeneous neuronal membranes regarding the preference of protein membrane orientation.⁵⁹

Our study also suggests an interesting insertion stabilization mechanism of $\text{A}\beta$ in membrane. With the peptide in an initial orientation in which the Lys-28 is at the lipid–water interface and the C-terminus at the lipid bilayer center, we observed Lys-28 snorkeling.^{60,61} In all of the inserted states observed in this study, the lysine residue stretched to the charged region to the negatively charged PC phosphorus or in few cases to the 3- β -hydroxyl polar group of cholesterol (Figures 5 and 13). In addition, the negatively charged C-terminus was found to anchor to the positively charged PC nitrogen (Figures 2 and 5). This intriguing dual-docking mechanism, lysine snorkeling to the upper layer and C-terminus anchoring to the lower layer, appears to stabilize the fully inserted protein orientation. This protein insertion–stabilization mechanism might operate in the neuronal membrane *in vivo* to keep the newly released protein in the

inserted state upon its release by the secretases. An interesting implication inferred from this simulation study is that cholesterol essentially doubles the insertion efficiency of the peptide, that is, from 25 to 50% for $\text{A}\beta_{40}$ (A-C series) and 50% to 100% for $\text{A}\beta_{42}$ (B-D series). Of course, determining the true insertion efficiency will require more replicates and longer observation time. Note that previous experimental work has indicated that cholesterol strongly promotes $\text{A}\beta_{40}$ insertion in saturated PC bilayers.⁷

Protein folding/unfolding events of the LID and non-LID in the cholesterol-depleted and enriched membranes were examined by calculating the percentages of ordered structures, α -helix and β -sheet in the two protein domains (Table 1). The LID is a unique peptide domain that begins with a positively charged Lys-28, followed by a region of highly hydrophobic and neutral segment, and then ends with a negatively charged C-terminus. The non-LID, on the other hand, is charged and polar. Therefore, the non-LID interacts exclusively with the polar region of the membranes whereas the LID interacts with the lipid acyl chains only when the peptide is in the inserted state (Figure 2). We observed prominent membrane surface-assisted protein folding in the PC membrane only. There, random coil-to- β -sheet transition occurred in the non-LID of $\text{A}\beta_{40}$ for replicates A3 and A4, two of the three observed surface states for $\text{A}\beta_{40}$. This result suggests that the highly disordered cholesterol-depleted lipid domain provides a favorable surface for the non-LID to interact with the polar region of the membrane. This gives rise to the highly structured β -sheet on the membrane surface. This

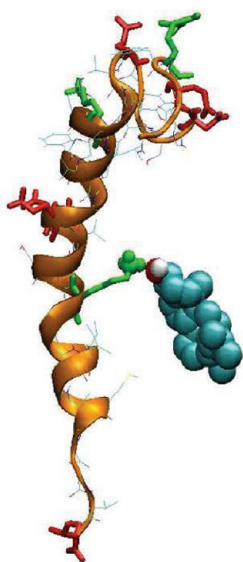


Figure 13. Demonstration of the close contact between cholesterol and Lys-23 of $\text{A}\beta_{40}$ in cholesterol-enriched lipid domains. The cholesterol is represented by van der Waals spheres. A close contact between the Lys-23 of $\text{A}\beta_{40}$ and the 3- β hydroxyl group of cholesterol is clearly observed. See the legend of Figure 1 for details of the protein representation.

structured motif of the protein might represent a 2D surface-template⁶ for the formation of the $\text{A}\beta$ oligomers by recruiting other $\text{A}\beta$ peptides either in the membrane or from the aqueous phase. More simulation and experimental studies are needed to confirm this membrane event.

Interestingly, the longer and more hydrophobic peptide, $\text{A}\beta_{42}$, exhibited only the inserted orientation in the absence of cholesterol, and the non-LID showed no protein folding on the membrane surface (Table 1). This behavior demonstrates the importance of the protein membrane orientation in protein folding on the cholesterol-depleted membrane surface. In the highly ordered PC/CHOL bilayers, the appearance of unstable β -sheets was found for both the non-LID and the LID of $\text{A}\beta_{40}$. There were fewer β -sheets in the non-LID of $\text{A}\beta_{42}$, and they were less stable. These observations indicate that the highly ordered environment of cholesterol-enriched membranes might promote some unstable β -sheet formation within our current 200 ns simulation time. We do not know whether these unstable β -sheets will dissipate or form stable β -sheets. This awaits future exploration.

In addition to protein folding to β -sheets, we observed protein unfolding from a structured α -helix to random coil of both non-LID and LID. There was little protein unfolding in the surface state for either the non-LID or the LID when compared with the inserted state. In addition, for the inserted state, the extent of the unfolding in the non-LID was consistently smaller than that in the LID. At most, 46% of the helix unfolded (non-LID of C3). Unfolding in the LID varied widely, from a slight increase in the helix content for A1 to 0% helix, or complete unfolding, in C2. These observations suggest that partial unfolding of the LID of a newly released $\text{A}\beta$ is likely to occur rapidly within the structurally homogeneous and hydrophobic acyl chain region of the neuronal membranes. However, the non-LID is likely to unfold more slowly on the more structurally complex polar lipid headgroup region. More replicates and much longer simulations are needed

to identify the role of cholesterol in modulating the partial folding of the non-LID and LID of the peptide. However, our cholesterol interaction dynamics results (Figures 11–13) suggest that cholesterol exerts its effects mainly by aligning the PC acyl chains or via the condensing effect^{13,14} rather than by direct contact with the protein.

The protein-induced membrane disruption was measured by eight membrane parameters: surface area per lipid (A_p and A_c), transbilayer thickness (z_p , z_c , and z_w), and lipid order (S_{p1} , S_{p2} , and S_c). These parameters were calculated for the ALs and nALs of the cholesterol-depleted and enriched membranes. Although the selection of the 0.5 nm cutoff in selecting the AL and nALs is somehow arbitrary, it provides a useful length scale standard to compare the protein-induced effects between two peptides of different lengths and membranes of different cholesterol contents.

Overall both $\text{A}\beta_{40}$ and $\text{A}\beta_{42}$ significantly increased the surface area of PC in PC and PC/CHOL bilayers (Figure 6) upon comparing the measurements in ALs versus nALs. Only a modest increase in the PC surface area was induced by the protein in PC bilayers. However, a larger increase in the PC surface area by the protein was found in PC/CHOL bilayers. $\text{A}\beta_{40}$ appeared to perturb the PC surface area slightly more than $\text{A}\beta_{42}$ (Figure 6) probably due to the hydrophobic mismatch between the shorter $\text{A}\beta_{40}$ and the thicker PC/CHOL bilayer versus the longer $\text{A}\beta_{42}$ and the thicker PC/CHOL. No significant change however was observed in the surface area of cholesterol. This observation suggests that the surface area of cholesterol as calculated by the current method is not a sensitive indicator of protein-induced disruption of membrane structures. Future work on the development of a more accurate method for cholesterol surface determination is still needed to address this issues.

Interestingly the extent of protein-induced decline in the average z_p and, particularly, z_w of $\text{A}\beta_{42}$ in PC (B series) ranked the highest among the other three systems (A, C, and D series). This observation suggests stronger membrane disruption of $\text{A}\beta_{42}$ in cholesterol-depleted membranes. In addition, the larger protein-induced decline in z_w , an important noninvasive marker of membrane disruption, found in the B series agrees with the observation that that $\text{A}\beta_{42}$ is more neurotoxic than $\text{A}\beta_{40}$ in cell studies.³ Our study further suggests that most membrane disruption was associated with $\text{A}\beta_{42}$ in cholesterol-depleted membranes and that the presence of cholesterol (C and D series) significantly increased the water barrier thickness when compared with the case of no cholesterol (A and B series). This indicates a protective effect of cholesterol in preventing membrane disruption. A similar observation of cholesterol-induced reduction of water influx inside the acyl chain region was also found in a recent study on dimyristoyl-PC (DMPC) and DMPC/CHOL bilayers.¹⁷

Finally, the average S_c provides a useful marker for the effect of protein on the sterol orientation in membranes. Here, a larger protein-induced 32% drop in the S_c of the upper layer for $\text{A}\beta_{40}$ than for $\text{A}\beta_{42}$ in PC/CHOL bilayers may indicate a stronger membrane disruptive effect of $\text{A}\beta_{40}$ versus $\text{A}\beta_{42}$ in cholesterol-enriched membranes. This differential effect may again be related to the hydrophobic length mismatch of the shorter protein placed in a thicker cholesterol-containing membranes. This also agrees with the stronger perturbation effect of $\text{A}\beta_{40}$ on PC surface area discussed above. Interestingly, this mismatch may also explain the presence of partially inserted state for $\text{A}\beta_{40}$ when only the fully inserted state existed for $\text{A}\beta_{42}$. This would reflect

the higher energy requirement of stretching the shorter protein in a thicker bilayer.

5. CONCLUSIONS

In conclusion, our simulation study provides a systematic survey of the membrane interaction events of the $\text{A}\beta$ peptides in cholesterol-depleted and enriched membranes based on the 200 ns simulation replicates. The protective role of cholesterol in preventing β -sheet formation and the membrane disruption provides some molecular-based insights of the early membrane interaction events of the newly released $\text{A}\beta$ from secretases that might be associated with the pathogenesis of AD.

■ ASSOCIATED CONTENT

5 Supporting Information. Details of mathematical procedures for the determination of the AL column and the nAL region (S1), the calculation of cross-section area (A) of AL column and nAL region (S2), and the calculation of particle number ($N_i(z)$) (S3). Also given are representative number density profile plots of lipid and water in PC and PC/CHOL in the presence or absence of protein (S4–S7), comparisons of order parameter of PC acyl chains in nALs and in pure bilayers (S8–S9), and time evolution of X_{CHOL} in ALs and nALs (S10) of PC and PC/CHOL bilayers. This material is available free of charge via the Internet at <http://pubs.acs.org>.

■ AUTHOR INFORMATION

Corresponding Author

*Address all correspondence to Kwan Hon Cheng, Texas Tech University, Science 101, Department of Physics, P.O. Box 41051, Lubbock, Texas 79409-1051, United States. E-mail: kelvin.cheng@ttu.edu. Tel.: 806-742-3767. Fax: 806-742-1182.

■ ACKNOWLEDGMENT

This work was supported by the Robert A. Welch Research Foundation grant (D-1158) and NIH grant (RC1GM090897-02) given to K.H.C.

■ REFERENCES

- (1) Sims, I. *Alzheimer's Dement.* **2009**, *5*, 234–270.
- (2) Roberson, E. D.; Mucke, L. *Science* **2006**, *314*, 781–784.
- (3) Selkoe, D. J. *Neuron* **1991**, *6*, 487–498.
- (4) Haass, C.; Schlossmacher, M. G.; Hung, A. Y.; Vigo-Pelfrey, C.; Mellon, A.; Ostaszewski, B. L.; Lieberburg, I.; Koo, E. H.; Schenk, D.; Teplow, D. B.; et al. *Nature* **1992**, *359*, 322–325.
- (5) Skovronsky, D. M.; Lee, V. M.; Trojanowski, J. Q. *Annu. Rev. Pathol.* **2006**, *1*, 151–170.
- (6) Bokvist, M.; Lindstrom, F.; Watts, A.; Grobner, G. *J. Mol. Biol.* **2004**, *335*, 1039–1049.
- (7) Ji, S. R.; Wu, Y.; Sui, S. F. *J. Biol. Chem.* **2002**, *277*, 6273–6279.
- (8) Terzi, E.; Holzemann, G.; Seelig, J. *J. Mol. Biol.* **1995**, *252*, 633–642.
- (9) Hardy, J. A.; Higgins, G. A. *Science* **1992**, *256*, 184–185.
- (10) Kremer, J. J.; Pallitto, M. M.; Sklansky, D. J.; Murphy, R. M. *Biochemistry* **2000**, *39*, 10309–10318.
- (11) Coles, M.; Bicknell, W.; Watson, A. A.; Fairlie, D. P.; Craik, D. J. *Biochemistry* **1998**, *37*, 11064–11077.
- (12) Luhrs, T.; Ritter, C.; Adrian, M.; Riek-Lohr, D.; Bohrmann, B.; Dobeli, H.; Schubert, D.; Riek, R. *Proc. Natl. Acad. Sci. U.S.A.* **2005**, *102*, 17342–17347.
- (13) Niemela, P. S.; Hyvonen, M. T.; Vattulainen, I. *Biochim. Biophys. Acta* **2009**, *1788*, 122–135.
- (14) Niemela, P. S.; Ollila, S.; Hyvonen, M. T.; Karttunen, M.; Vattulainen, I. *PLoS Comput. Biol.* **2007**, *3*, 304–312.
- (15) Somerharju, P.; Virtanen, J. A.; Cheng, K. H.; Hermansson, M. *Biochim. Biophys. Acta* **2009**, *1788*, 12–23.
- (16) Khelashvili, G.; Pabst, G.; Harries, D. *J. Phys. Chem. B* **2010**, *114*, 7524–7534.
- (17) Khelashvili, G.; Mondal, S.; Andersen, O. S.; Weinstein, H. *J. Phys. Chem. B* **2010**, *114*, 12046–12057.
- (18) Davis, C. H.; Berkowitz, M. L. *J. Phys. Chem. B* **2009**, *113*, 14480–14486.
- (19) Davis, C. H.; Berkowitz, M. L. *Biophys. J.* **2009**, *96*, 785–797.
- (20) Davis, C. H.; Berkowitz, M. L. *Proteins* **2010**, *78*, 2533–2545.
- (21) Devanathan, S.; Salamon, Z.; Lindblom, G.; Grobner, G.; Tollin, G. *FEBS J.* **2006**, *273*, 1389–1402.
- (22) Lemkul, J. A.; Bevan, D. R. *Arch. Biochem. Biophys.* **2008**, *470*, 54–63.
- (23) Lemkul, J. A.; Bevan, D. R. *FEBS J.* **2009**, *276*, 3060–3075.
- (24) Lemkul, J. A.; Bevan, D. R. *Biochemistry* **2010**, *49*, 3935–3946.
- (25) Lemkul, J. A.; Bevan, D. R. *J. Phys. Chem. B* **2010**, *114*, 1652–1660.
- (26) Xu, Y.; Shen, J.; Luo, X.; Zhu, W.; Chen, K.; Ma, J.; Jiang, H. *Proc. Natl. Acad. Sci. U.S.A.* **2005**, *102*, 5403–5407.
- (27) Anderson, R. G.; Jacobson, K. *Science* **2002**, *296*, 1821–1825.
- (28) Gallegos, A. M.; Storey, S. M.; Kier, A. B.; Schroeder, F.; Ball, J. M. *Biochemistry* **2006**, *45*, 12100–12116.
- (29) Pugliali, L.; Friedlich, A. L.; Setchell, K. D.; Nagano, S.; Opazo, C.; Cherny, R. A.; Barnham, K. J.; Wade, J. D.; Melov, S.; Kovacs, D. M.; Bush, A. I. *J. Clin. Invest.* **2005**, *115*, 2556–2563.
- (30) Simons, K.; Ikonom, E. *Science* **2000**, *290*, 1721–1726.
- (31) Wang, M. M.; Olsher, M.; Sugar, I. P.; Chong, P. L. *Biochemistry* **2004**, *43*, 2159–2166.
- (32) Pan, J.; Tristram-Nagle, S.; Nagle, J. F. *Phys. Rev. E* **2009**, *80*, 021931.
- (33) Tristram-Nagle, S.; Chan, R.; Kooijman, E.; Uppamoochikkal, P.; Qiang, W.; Weliky, D. P.; Nagle, J. F. *J. Mol. Biol.* **2010**, *402*, 139–153.
- (34) Zhu, Q.; Cheng, K. H.; Vaughn, M. W. *J. Phys. Chem. B* **2007**, *111*, 11021–11031.
- (35) Bekker, H.; Berendsen, H. J. C.; Dijkstra, E. J.; Achterop, S.; van Drunen, R.; van der Spoel, D.; Sijbers, A.; Keegstra, H.; Reitsma, B.; Renardus, M. K. R. *Gromacs: A Parallel Computer for Molecular Dynamics Simulations*. In *Physics Computing 92*; World Scientific: Singapore, 1993.
- (36) Berendsen, H. D.; van der Spoel, D.; van Drunen, R. *Comput. Phys. Commun.* **1995**, *91*, 43–56.
- (37) Lindahl, E.; Hess, B.; van der Spoel, D. *J. Mol. Model.* **2001**, *7*, 306–317.
- (38) Van Der Spoel, D.; Lindahl, E.; Hess, B.; Groenhof, G.; Mark, A. E.; Berendsen, H. J. J. *Comput. Chem.* **2005**, *26*, 1701–1718.
- (39) Holtje, M.; Forster, T.; Brandt, B.; Engels, T.; von Rybinski, W.; Holtje, H. D. *Biochim. Biophys. Acta* **2001**, *1511*, 156–167.
- (40) Berendsen, H. J. C.; Postma, J. P. M.; van Gunsteren, W. F.; Hermans, J. *Interaction Models for Water in Relation to Protein Hydration*. In *Intermolecular Forces*; Pullman, B., Ed.; Reidel: Dordrecht, The Netherlands, 1981; pp 331–342.
- (41) Hess, B.; Bekker, H.; Berendsen, H. J. C.; Fraaije, J. G. E. M. *J. Comput. Chem.* **1997**, *18*, 952–962.
- (42) van der Spoel, D.; Lindahl, E.; Hess, B.; van Buuren, A. R.; Apol, E.; Meulenhoff, P. J.; Tielemans, D. P.; Sijbers, A. L. T. M.; Feenstra, K. A.; van Drunen, R.; Berendsen, H. J. C. *Gromacs User Manual*, version 4.0; <http://www.gromacs.org>, 2005.
- (43) Darden, T.; York, D.; Pedersen, L. *J. Chem. Phys.* **1993**, *98*, 10089–10092.
- (44) Essmann, U.; Perera, L.; Berkowitz, M. L.; Darden, T.; Lee, H.; Pedersen, L. *J. Chem. Phys.* **1995**, *103*, 8577–8593.
- (45) Hockney, R. W.; Goel, S. P.; Eastwood, J. W. *J. Comput. Phys.* **1974**, *14*, 148–158.

- (46) Bussi, G.; Donadio, D.; Parrinello, M. *J. Chem. Phys.* **2007**, *126*, 014101.
- (47) Hess, B.; Kutzner, C.; van der Spoel, D.; Lindahl, E. *J. Chem. Theory Comput.* **2008**, *4*, 435–447.
- (48) Berendsen, H. J. C.; Postma, J. P. M.; van Gunsteren, W. F.; DiNola, A.; Haak, J. R. *J. Chem. Phys.* **1984**, *81*, 3684–3690.
- (49) Lee, A. G. *Biochim. Biophys. Acta* **2003**, *1612*, 1–40.
- (50) Warren, G. B.; Houslay, M. D.; Metcalfe, J. C.; Birdsall, N. J. *Nature* **1975**, *255*, 684–687.
- (51) Hofäss, C.; Lindahl, E.; Edholm, O. *Biophys. J.* **2003**, *84*, 2192–2206.
- (52) Fishman, G. S. *Monte Carlo: Concepts, Algorithms, and Applications*; Springer-Verlag: New York, 1997.
- (53) Alwarawrah, M.; Dai, J.; Huang, J. *J. Phys. Chem. B* **2010**, *114*, 7516–7523.
- (54) Center for Molecular and Biomolecular Bioinformatics homepage. <http://www.cmbi.ru.nl> (accessed May 2009), updated CMBI version by ElmK, April 1, 2000.
- (55) Kabsch, W.; Sander, C. *Biopolymers* **1983**, *22*, 2577–2637.
- (56) Kraulis, P. J. *J. Appl. Crystallogr.* **1991**, *24*, 946–950.
- (57) Merritt, E. A.; Bacon, D. J. *Methods Enzymol.* **1997**, *277*, 505–524.
- (58) Humphrey, W.; Dalke, A.; Schulten, K. *J. Mol. Graph.* **1996**, *14*, 33–38.
- (59) Simons, K.; Ehehalt, R. *J. Clin. Invest.* **2002**, *110*, 597–603.
- (60) Jaud, S.; Fernandez-Vidal, M.; Nilsson, I.; Meindl-Beinker; Hubner, N. C.; Tobias, D. J.; von Heijne, G.; White, S. H. *Proc. Natl. Acad. Sci. U.S.A.* **2009**, *106*, 11588–11593.
- (61) Strandberg, E.; Killian, J. A. *FEBS Lett.* **2003**, *544*, 69–73.